**Supplemental Data**

**Supplemental Methods**

**Generation of *Gfap-Cre*$^{Tg}$ mice.**

In a search for a bacterial artificial chromosome (BAC) clone that contains the murine *Gfap* (glial fibrillary acidic protein) locus, we found that BAC clone RP23-463E7 covers 198.4 kb of chromosome 11 containing a 130.3-kb 5′ upstream genomic sequence and a 59.6-kb 3′ downstream genomic sequence along with the entire murine *Gfap* locus. Clone RP23-463E7 was assumed to include all expression control sequences that drive the murine *Gfap* gene. Using the Red/ET recombination technology (1), we replaced the translation initiation codon of *Gfap* in the BAC clone with the entire *Cre* cDNA sequence, which includes an N-terminal nuclear localization sequence and a *βGlobin*-derived poly A sequence; this replacement was done so as to be precisely in-frame. Thus, we obtained a recombinant BAC expression vector encoding the *Cre* gene including the 5′ upstream and 3′ downstream genomic sequences of the murine *Gfap* locus. We microinjected this expression vector into C57BL/6J fertilized eggs to generate *Gfap-Cre*$^{Tg}$ mice.

**Generation of *Aclp*$^{HSC\text{-}KO}$ mice.**

The targeting vector was designed to target exons 7–20 of the *Aclp* gene by using CRE recombinase. A neomycin-resistance cassette with flippase recognition target (FRT) sites on both sides and a *loxP* site were inserted at intron 6, while a *loxP* site was inserted at intron 20. A diphtheria toxin A cassette (DTA) was ligated into the 3′ end of the targeting vector (Supplemental Figure 3A), which was electroporated into C57BL/6J-derived embryonic stem cells (C57BL/6 ES cells) after being *Mlu*I-linearized. Following positive and negative selection, southern blot analysis using 5′ and 3′ probes was employed to select ES cell clones in which homologous recombination had occurred (Supplemental Figure 3B). These ES cell clones were injected into BALB/c-derived blastocysts to obtain chimeric mice. These chimeric mice were bred with C57BL/6J mice to obtain F1 generation mice that had achieved germline transmission and possessed targeted alleles (Supplemental Figure 3C). We bred the F1 generation mice with Tg mice (C57BL/6 background) expressing FLP recombinase under the control of a CAG promoter to obtain mice possessing floxed allele with the neomycin resistance cassette removed. These mice were then bred with C57BL/6J mice to remove the FLP transgene, while further breeding was conducted to obtain *Aclp*$^{fl/fl}$

mice homozygous for floxed alleles (Supplemental Figure 3D). *Gfap-Cre*$^{Tg}$ mice were further bred to obtain HSC-specific ACLP-knockout (*Aclp*$^{HSC\text{-}KO}$) mice. The *Aclp*$^{HSC\text{-}KO}$ mice were bred with collagen 1α1 promoter-DKK-1 Tg mice (2) (*Dkk-1*$^{Tg}$ mice, provided by Dr. Henry M. Kronenberg) to generate double-mutant (*Aclp*$^{HSC\text{-}KO}$*Dkk-1*$^{Tg}$) mice.

**Biochemical analysis.**

Serum ALT, total cholesterol, TG, and glucose were determined as previously described (3). Serum insulin was measured using a mouse insulin ELISA kit (Mercodia AB, Uppsala, Sweden). Serum leptin and IL-6 were determined using mouse or human leptin and IL-6 quantikine ELISA kits, respectively (R&D Systems). Serum concentrations of free fatty acid (FFA) were measured using LabAssay NEFA (Wako Pure Chemical Industries). Hepatic TG content was measured as previously described (3).

**Deglycosylation of rACLP.**

rACLP was deglycosylated using Deglycosylation Mix (New England Biolabs Japan Inc., Tokyo, Japan). Solvent containing 600 ng of dissolved purified recombinant ACLP

was substituted with deglycosylation buffer (0.1 M Tris-HCl, 1% CHAPS, pH 8.6 at 37°C), and the final volume was adjusted to 35 μl. Deglycosylation enzyme mix (5 μl) was added, followed by inversion mixing at 37°C for 4 hr. After centrifugation at 15,000 × *g* and 4°C for 10 min, the supernatant was used in western blotting using anti-ACLP antibody.

**PPARγ promoter activity assay.**

An expression vector (provided by Dr. Makoto Seo) with a luciferase gene downstream of the human PPARγ promoter was transfected into murine ACLP-deficient HSCs using Lipofectamine LTX. At 24 hr after transfection, rACLP (100 ng/ml), DKK-1 (20 ng/ml), FZD8CRD (20 μg/ml), or anti-ACLP antibody (10 μg/ml) was added to the HSCs, which were then cultured for 12 hr. Intracellular expression of luciferase was quantified using the Dual-Luciferase Reporter Assay System (Promega Corporation, Madison, WI, USA). Cells were lysed with a Passive Lysis Buffer included with the kit, Luciferase Assay Reagent II was added to the cell lysate, and the resulting chemiluminescence was measured with a TD-20/20 Luminometer (Turner BioSystems, Sunnyvale, CA, USA).

**Quantitative reverse-transcription (qRT-) PCR analysis.**

We isolated and purified RNA from liver tissues and cells using an RNeasy Mini Kit or RNeasy Micro Kit (Qiagen, Dusseldorf, Germany). Reverse transcription was carried out with a High-Capacity cDNA Reverse Transcription Kit (Thermo Fisher Scientific) or WT-Ovation RNA Amplification System (NuGEN Technologies, Inc., San Carlos, CA, USA). Real-time PCR amplification was performed using a Thermal Cycler Dice Real Time System (Takara Bio, Otsu, Japan) as described (3).

**Preparation of vitamin A-coupled liposomes carrying ACLP-siRNA.**

ACLP-siRNA- or control-siRNA- bearing vitamin A-coupled liposomes were prepared as described (4), using ACLP-siRNA or control-siRNA (Nippon Gene, Tokyo, Japan) labeled with 6'-carboxyfluorescein (FAM, Ex/Em = 492/512 nm); liposomes containing cationic lipids (LipoTrust$^{TM}$ SR, Hokkaido System Science, Sapporo, Japan); and vitamin A (Sigma).

**Fluorescence-activated cell sorting (FACS) analysis.**

HSCs were isolated from mice. Multi-color FACS staining was conducted using combinations of the following antibodies: PE-conjugated anti-desmin antibody (Novus Biologicals, CO, USA); PE/Cy7-conjugated anti-CD45.2

antibody (Biolegend, CA, USA); APC/Cy7-conjugated anti-Thy1.1 antibody (Biolegend). Those stained cells were analyzed with BD FACSCanto II (BD Bioscience, CA, USA), using FlowJo software. $CD45.2^{-}Thy1.1^{-}FAM^{+}desmin^{+}$ cells were sorted by BD FACS Aria-II (BD Bioscience).

**Murine models of liver fibrosis.**

For the $CCl_4$ model, eight-week-old male $Aclp^{fl/fl}$ and $Aclp^{HSC\text{-}KO}$ mice (n = 4/group) were treated with $CCl_4$ at a dose of 5 μl (10% $CCl_4$ in corn oil)/g body weight, by intraperitoneal injection twice a week for 4 weeks, as previously described (5). For the BDL model, eight-week-old male $Aclp^{fl/fl}$ and $Aclp^{HSC\text{-}KO}$ mice (n = 7/group) were subjected to BDL or sham operation for 3 weeks. BDL was performed by ligating the common bile duct twice with silk sutures, as previously described (5).

**Supplemental References**


1. Zhang Y, Buchholz F, Muyrers JP, and Stewart AF. A new logic for DNA engineering using recombination in Escherichia coli. *Nat Genet.* 1998;20(2):123-8.

2. Guo J, Liu M, Yang D, Bouxsein ML, Saito H, Galvin RJ, et al. Suppression of Wnt signaling by Dkk1 attenuates PTH-mediated stromal cell response and new bone formation. *Cell Metab.* 2010;11(2):161-71.

3. Tomita K, Teratani T, Suzuki T, Shimizu M, Sato H, Narimatsu K, et al. Free cholesterol accumulation in hepatic stellate cells: mechanism of liver fibrosis aggravation in nonalcoholic steatohepatitis in mice. *Hepatology.* 2014;59(1):154-69.

4. Sato Y, Murase K, Kato J, Kobune M, Sato T, Kawano Y, et al. Resolution of liver cirrhosis using vitamin A-coupled liposomes to deliver siRNA against a collagen-specific chaperone. *Nat Biotechnol.* 2008;26(4):431-42.

5. Teratani T, Tomita K, Suzuki T, Oshikawa T, Yokoyama H, Shimamura K, et al. A high-cholesterol diet exacerbates liver fibrosis in mice via accumulation of free cholesterol in hepatic stellate cells. *Gastroenterology.* 2012;142(1):152-64

e10.

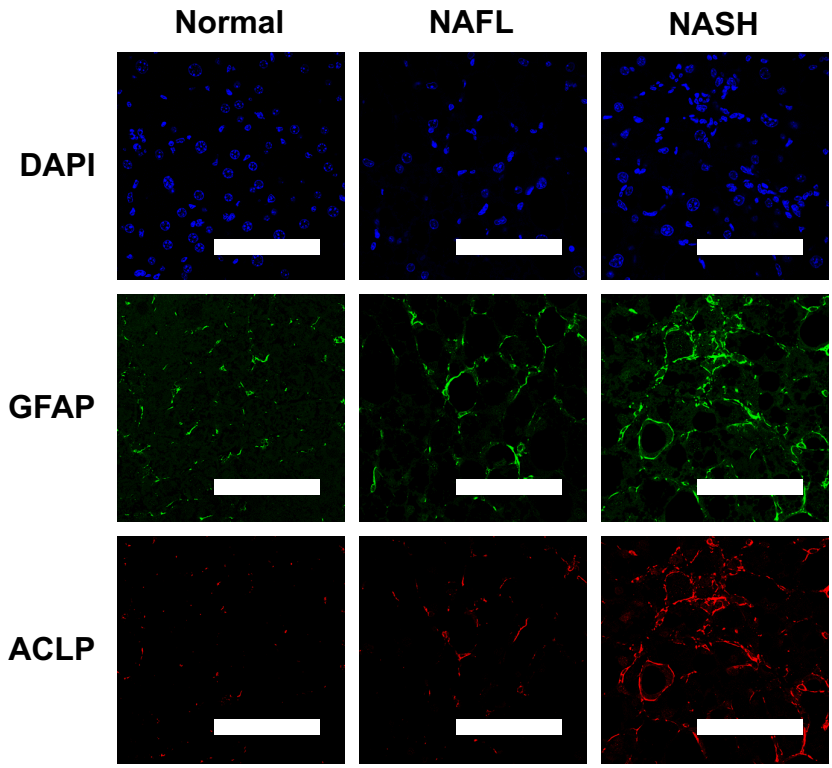


**Supplemental Figure 1. Immunofluorescence staining for ACLP and GFAP in liver samples from control subjects and NAFLD patients.**
Representative images of immunofluorescence staining for ACLP (red) and GFAP (green) in human liver tissue samples from controls (n = 14), NAFL patients (n = 16), and NASH patients (n = 44). The nuclei were stained with DAPI (blue). Scale bars: 100 μm. This figure is related to Figure 1A.

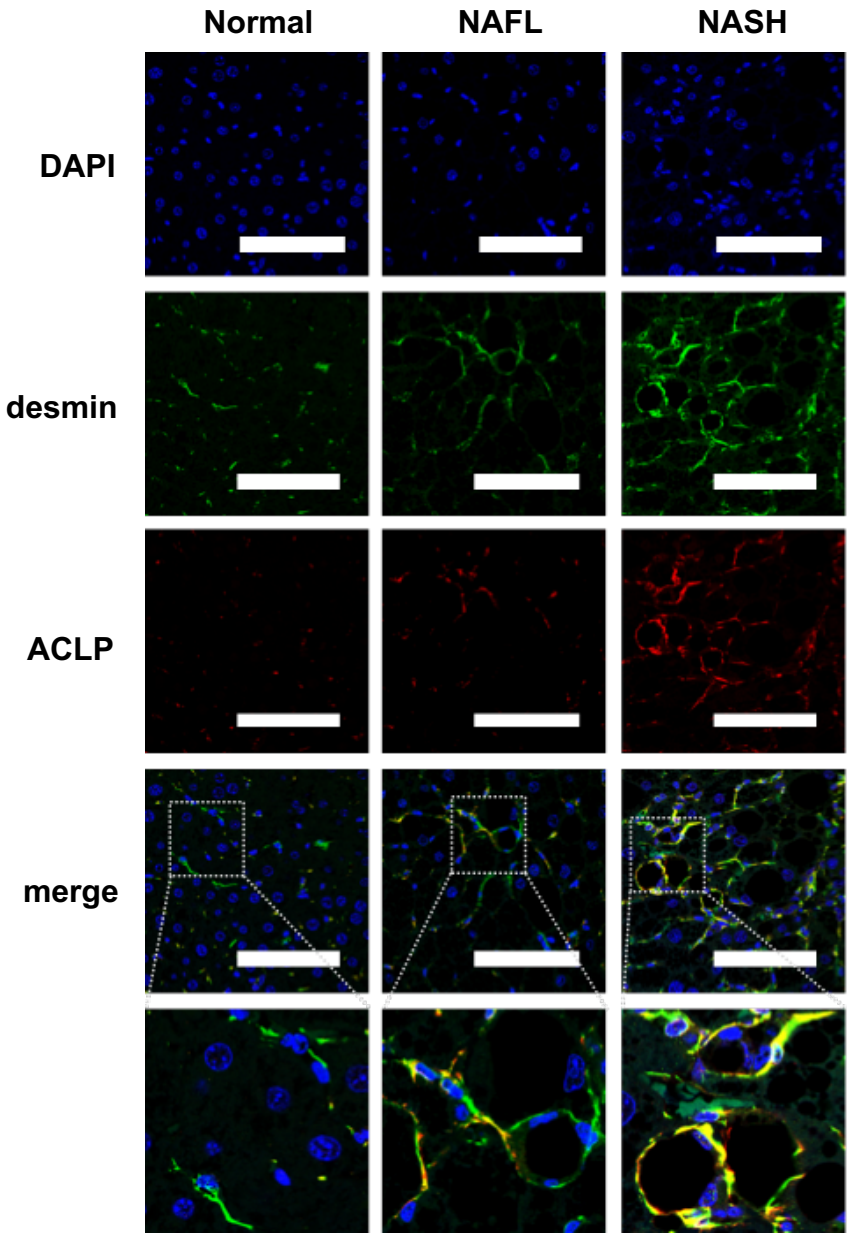


**Supplemental Figure 2. Immunofluorescence staining for ACLP and desmin in liver samples from control subjects and NAFLD patients.**
Representative images of immunofluorescence double staining for ACLP (red) and desmin (green) in human liver tissue samples from controls (n = 14), NAFL patients (n = 16), and NASH patients (n = 44). The co-stained sites are shown in yellow. The nuclei were stained with DAPI (blue). Scale bars: 100 μm.

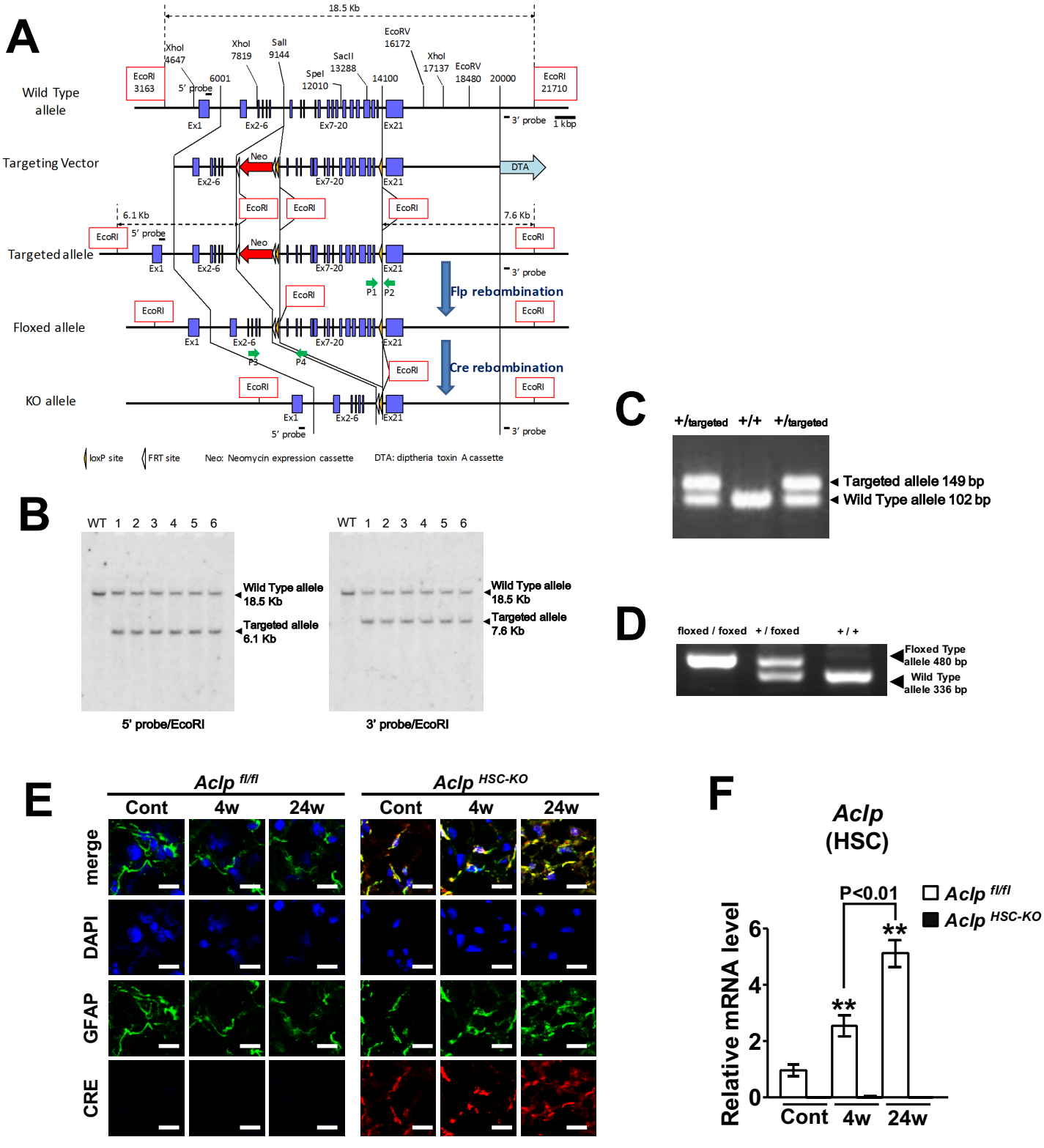


**Supplemental Figure 3. Preparation of HSC-specific ACLP-knockout mice.**

(A) Schemas of targeting vector and mutant alleles for preparing ACLP conditional knockout mice (see experimental procedures for details). (B) Southern blot analysis using a 5´ probe, a 3´ probe, and an *Eco*RI restriction DNA fragment to select six positive ES clones. (C) Following germline transmission, PCR genotyping using P1 and P2 primers was used to select mice harboring the targeted allele. (D) PCR genotyping using P3 and P4 primers to select $Aclp^{fl/fl}$ mice, $Aclp^{fl/+}$ mice, and $Aclp^{+/+}$ mice. (E, F) Eight-week-old male $Aclp^{fl/fl}$ and $Aclp^{HSC\text{-}KO}$ mice were fed an HFC diet for 4 weeks (n = 6/group) or 24 weeks (n = 9/group) to prepare NAFLD models or fed a control diet for 24 weeks (n = 6/group). (E) Immunofluorescence double staining of CRE (red) and GFAP (green) is shown. Co-stained sites are shown in yellow. The nuclei were stained with DAPI (blue). Scale bars: 10 μm. (F) *Aclp* mRNA expression in HSCs isolated from the livers. **p < 0.01 vs. HSCs in $Aclp^{fl/fl}$ mice fed a control diet. p-values obtained via one-way ANOVA with Tukey's post-hoc test. Error bars represent the SEM.

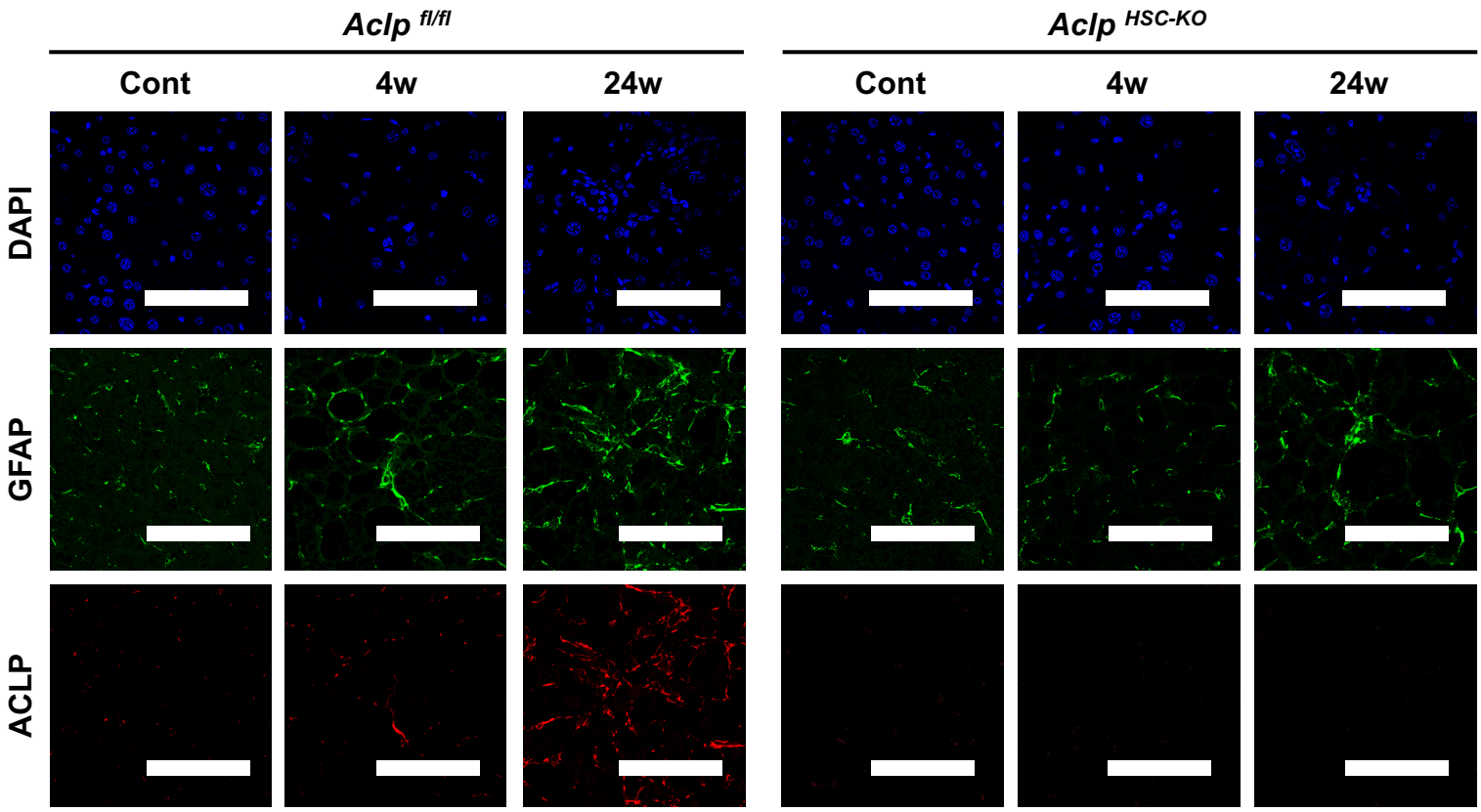


**Supplemental Figure 4. Immunofluorescence staining images of ACLP and GFAP in the livers of murine models of NAFLD.**
Eight-week-old male *Aclp*$^{fl/fl}$ and *Aclp*$^{HSC\text{-}KO}$ mice were fed an HFC diet for 4 weeks (n = 6/group) or 24 weeks (n = 9/group), or were fed a control diet for 24 weeks (n = 6/group). Representative images of immunofluorescence staining for ACLP (red) and GFAP (green) in murine liver sections. The nuclei were stained with DAPI (blue). Scale bars: 100 μm. This figure is related to Figure 1C.

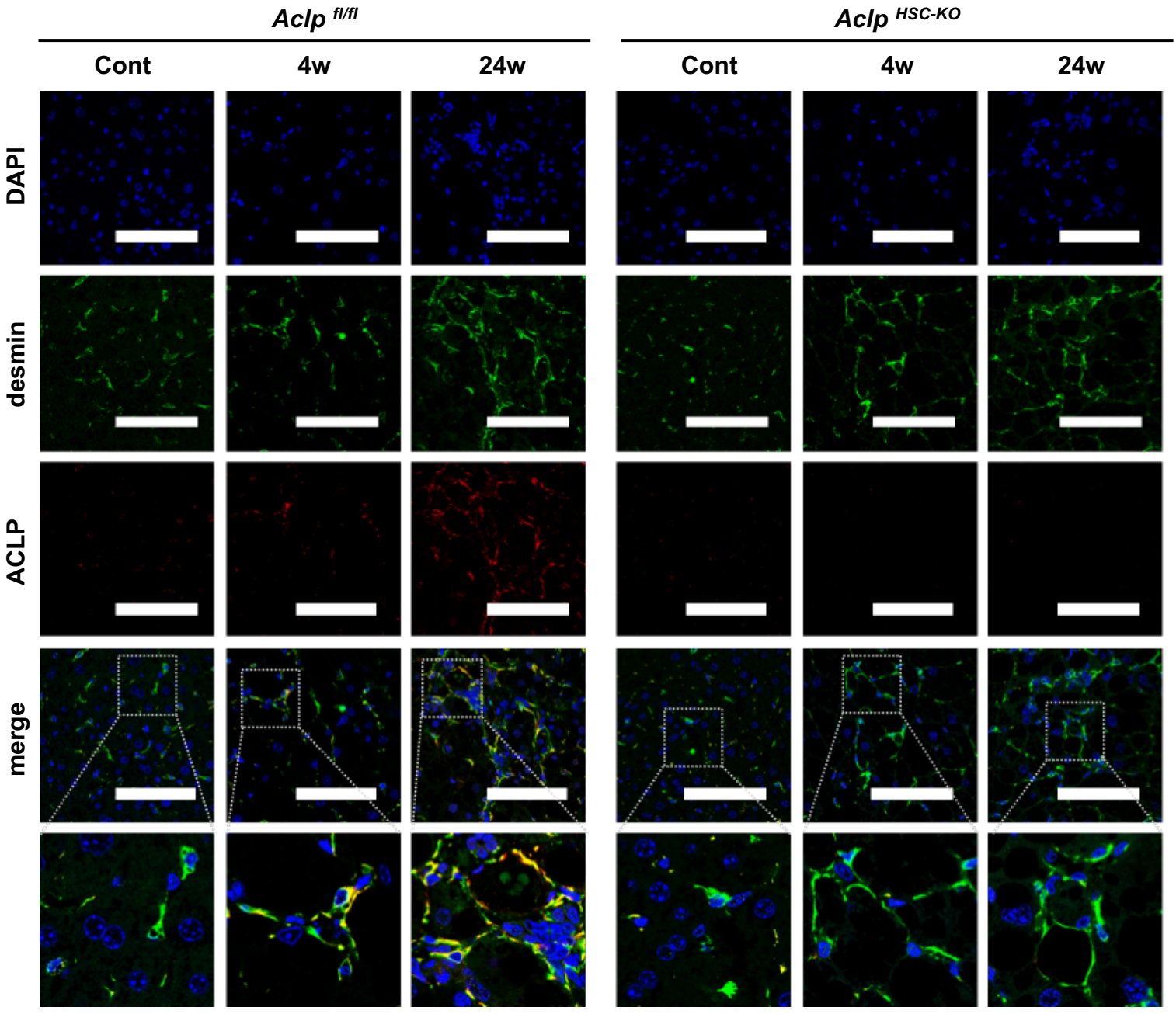


**Supplemental Figure 5. Immunofluorescence staining images of ACLP and desmin in the livers of murine models of NAFLD.**
Eight-week-old male *Aclp*$^{fl/fl}$ and *Aclp*$^{HSC\text{-}KO}$ mice were fed an HFC diet for 4 weeks (n = 6/group) or 24 weeks (n = 9/group), or were fed a control diet for 24 weeks (n = 6/group). Representative images of immunofluorescence double staining for ACLP (red) and desmin (green) in murine liver sections. Co-stained sites are shown in yellow. The nuclei were stained with DAPI (blue). Scale bars: 100 μm.

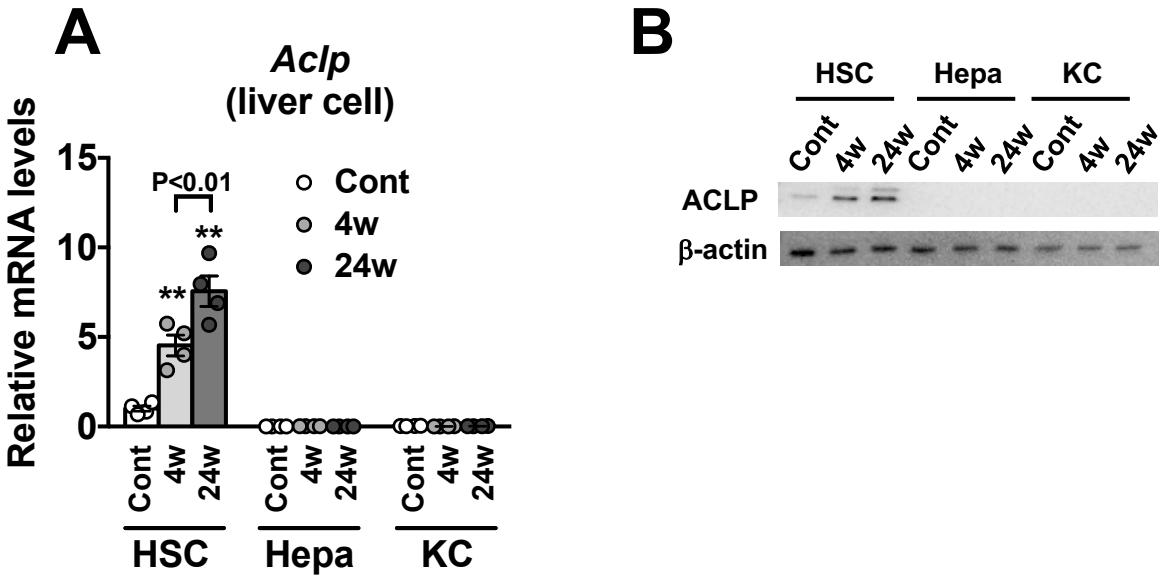


**Supplemental Figure 6. mRNA and protein expression of ACLP in hepatocytes and Kupffer cells in murine models of NAFLD.**
(A and B) Eight-week-old male *Aclp*$^{fl/fl}$ mice were fed an HFC diet for 4 or 24 weeks, or fed a control diet for 24 weeks (n = 4/group). (A) Quantification of *Aclp* mRNA expression in HSCs, hepatocytes, and Kupffer cells, isolated from these mice. **p < 0.01 vs. HSCs in *Aclp*$^{fl/fl}$ mice fed the control diet. (B) Western blot for ACLP expression in HSCs, hepatocytes, and Kupffer cells isolated from these mice. p-values obtained via one-way ANOVA with Tukey's post-hoc test. Error bars represent the SEM.

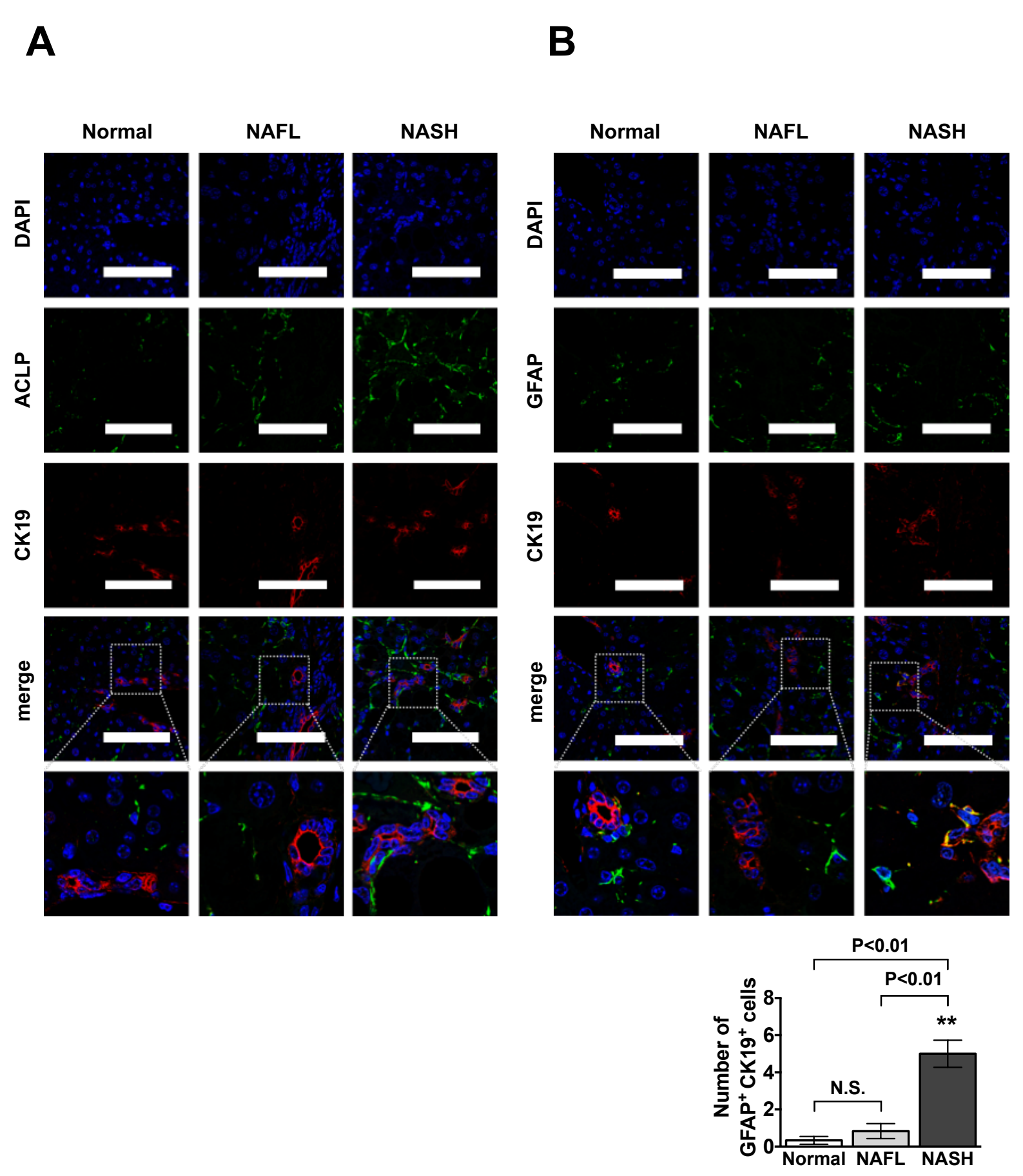


**Supplemental Figure 7. ACLP is not expressed in bile duct cells and ductular-appearing cells in human liver samples.**
(A) Representative images of immunofluorescence double staining for ACLP (green) and CK19, the marker of bile duct cells and ductular-appearing cells (red) in human liver tissue samples from controls (n = 14), NAFL patients (n = 16), and NASH patients (n = 44). The nuclei were stained with DAPI (blue). Scale bars: 100 µm. Co-stained sites could not be detected. (B) (Upper panel) Representative images of immunofluorescence double staining for GFAP (green) and CK19 (red) in human liver tissue samples from controls, NAFL patients, and NASH patients (n = 5/group). Co-stained sites are shown in yellow. The nuclei were stained with DAPI (blue). Scale bars: 100 µm. (Lower panel) Quantification of GFAP/CK19 double-positive cells (n = 5/group). Among the bile duct cells and ductular-appearing cells, we could detect just a few GFAP-positive cells, the number of which significantly increased in the livers of NASH patients, compared to control subjects. p-values obtained via one-way ANOVA with Tukey's post-hoc test. Error bars represent the SEM.

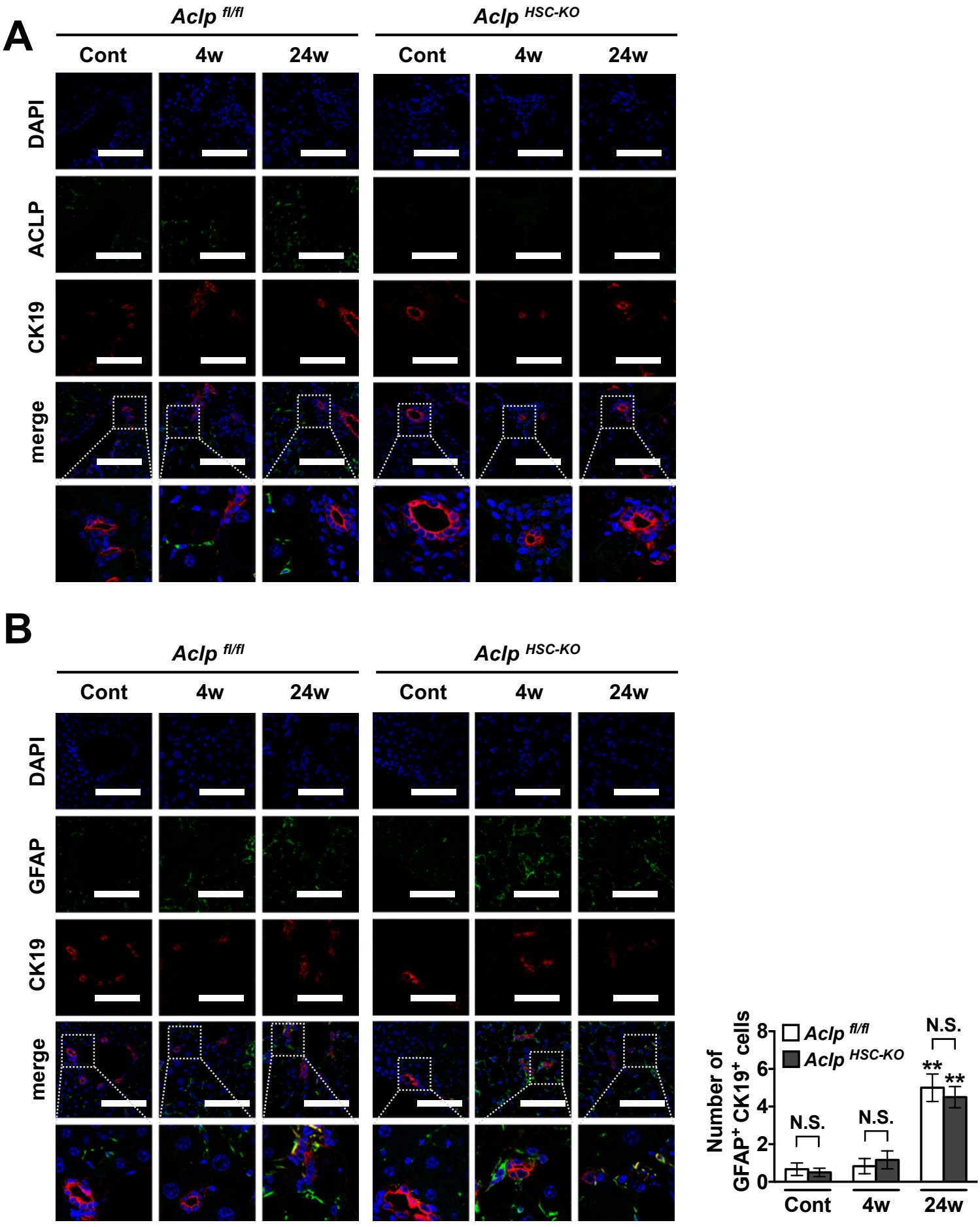
A
Aclp fl/fl
Aclp HSC-KO
Cont
4w
24w
Cont
4w
24w
DAPI
ACLP
CK19
merge
B
Aclp fl/fl
Aclp HSC-KO
Cont
4w
24w
Cont
4w
24w
DAPI
GFAP
CK19
merge
Number of GFAP+ CK19+ cells
Aclp fl/fl
Aclp HSC-KO
N.S.
N.S.
N.S.
**
**
0
2
4
6
8
Cont
4w
24w

**Supplemental Figure 8. ACLP is not expressed in bile duct cells and ductular-appearing cells in murine liver samples.**
(A and B) Eight-week-old male *Aclp*$^{fl/fl}$ and *Aclp*$^{HSC\text{-}KO}$ mice were fed an HFC diet for 4 or 24 weeks, or fed a control diet for 24 weeks (n = 5/group). (A) Representative images of immunofluorescence double staining for ACLP (green) and CK19 (red) in murine liver sections. The nuclei were stained with DAPI (blue). Scale bars: 100 μm. Co-stained sites could not be detected. (B) (Left panel) Representative images for immunofluorescence double staining for GFAP (green) and CK19 (red) in murine liver sections. Co-stained sites are shown in yellow. The nuclei were stained with DAPI (blue). Scale bars: 100 μm. (Right panel) Quantification of GFAP/CK19 double-positive cells. **$p < 0.01$ vs. *Aclp*$^{fl/fl}$ mice fed a control diet for 24 weeks. Among the bile duct cells and ductular-appearing cells, we could detect just a few GFAP-positive cells, the number of which significantly increased in the livers of NASH mice, compared to control mice. There was no significant difference in the number of those cells between *Aclp*$^{HSC\text{-}KO}$ and *Aclp*$^{fl/fl}$ mice. p-values obtained via one-way ANOVA with Tukey's post-hoc test. Error bars represent the SEM.

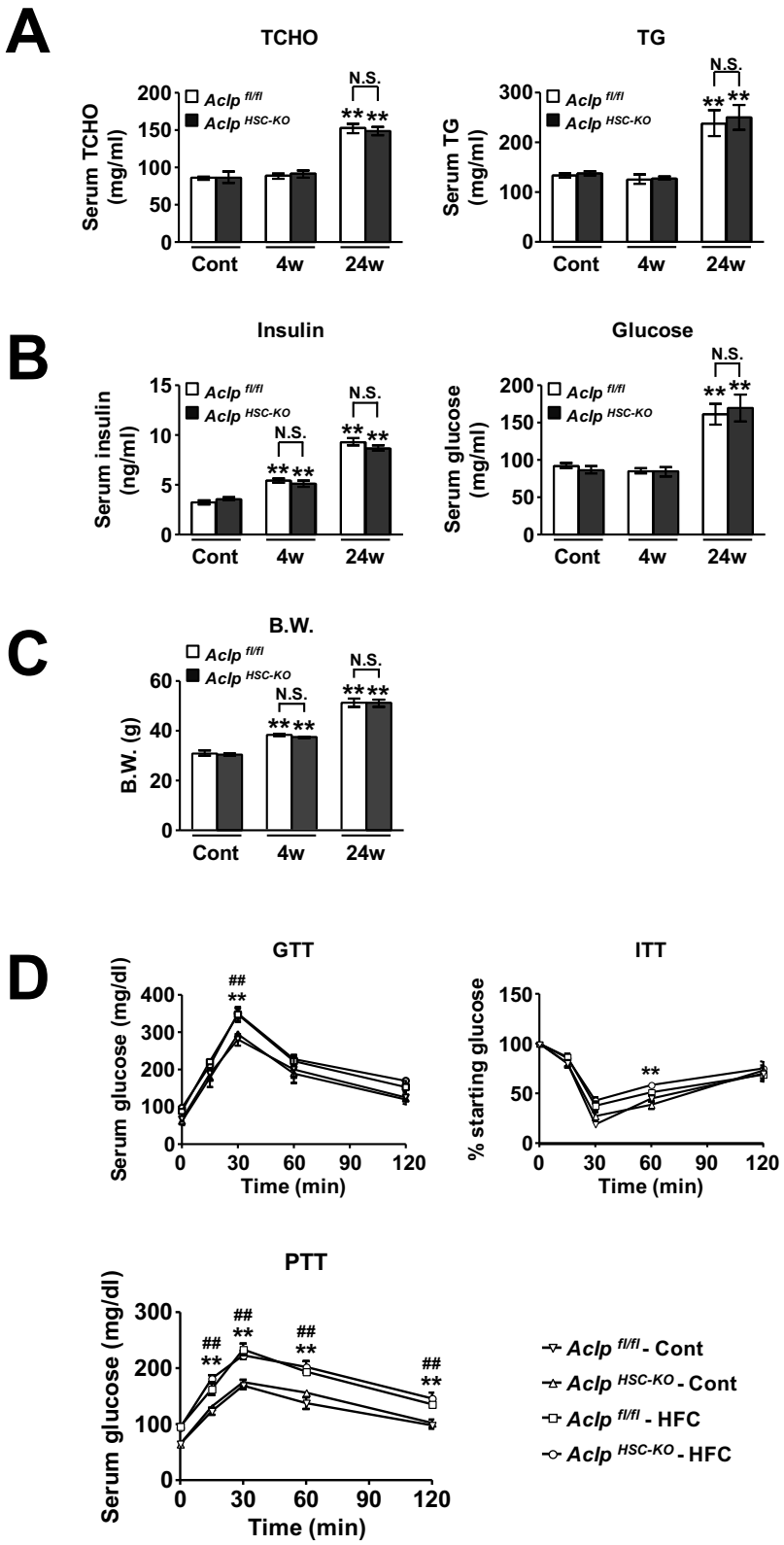


**Supplemental Figure 9. ACLP deficiency does not affect serum cholesterol, TG, glucose, or insulin levels in murine NAFLD.**
(A–D) Eight-week-old male *Aclp*$^{fl/fl}$ and *Aclp*$^{HSC\text{-}KO}$ mice were fed an HFC diet for 4 weeks (n = 6/group) or 24 weeks (n = 9/group) to prepare murine NAFLD models or fed a control diet for 24 weeks (n = 6/group). Serum levels of (A) total cholesterol and TG, and (B) insulin and glucose. (C) Body weight measurements. **p < 0.01 vs. *Aclp*$^{fl/fl}$ mice fed a control diet. (D) *Aclp*$^{fl/fl}$ and *Aclp*$^{HSC\text{-}KO}$ mice fed a control or HFC diet underwent GTT, ITT, and PTT at 21–23 weeks of their diets. **p < 0.01: *Aclp*$^{fl/fl}$-Cont vs. *Aclp*$^{fl/fl}$-HFC. $^{\#\#}$p < 0.01: *Aclp*$^{HSC\text{-}KO}$-Cont vs. *Aclp*$^{HSC\text{-}KO}$ -HFC. p-values obtained via one-way ANOVA with Tukey's post-hoc test. Error bars represent the SEM.

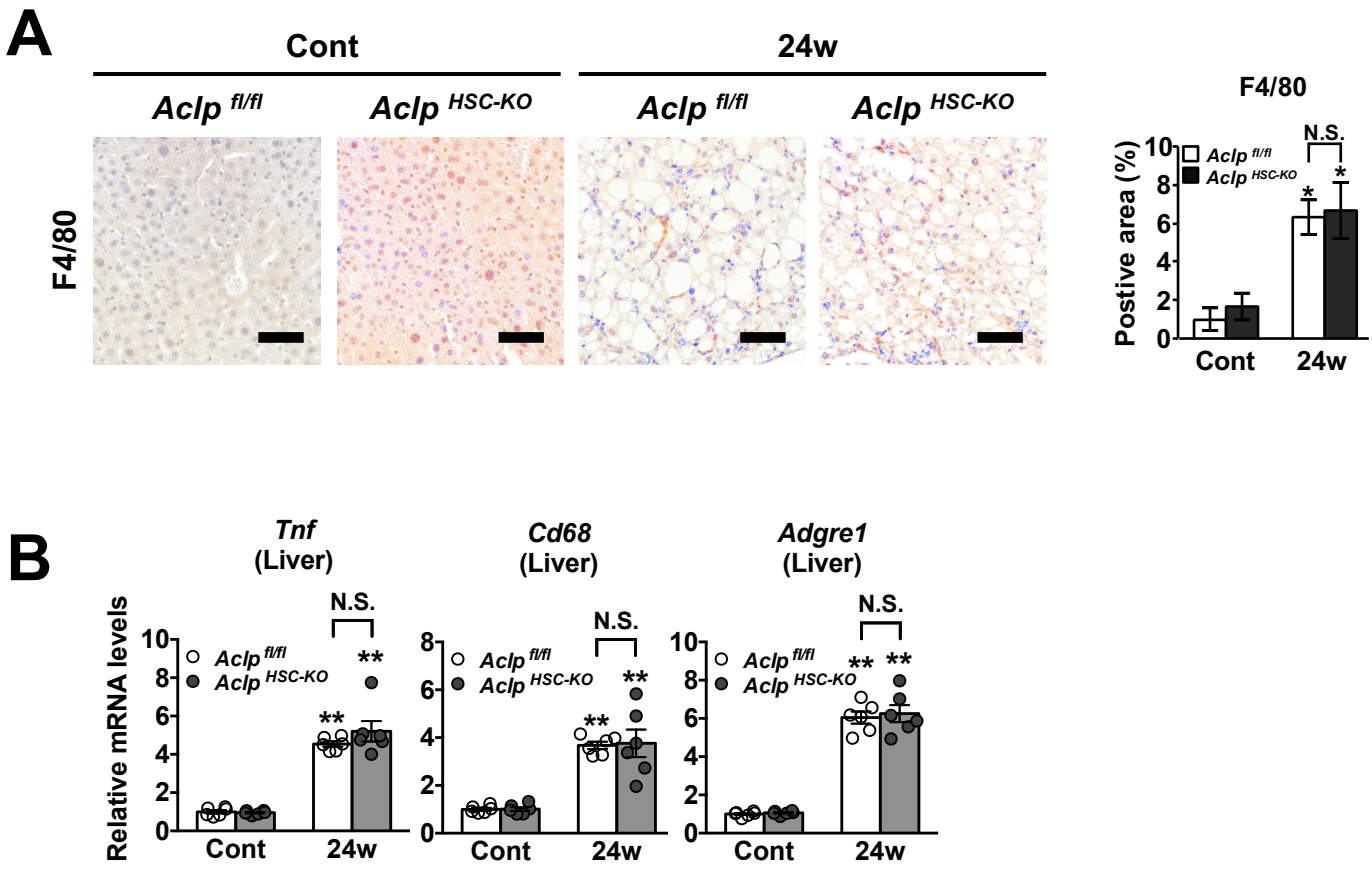


**Supplemental Figure 10. ACLP deficiency does not affect hepatic macrophage infiltration or Kupffer cell activation in murine NAFLD.**
(A and B) Eight-week-old male *Aclp*$^{fl/fl}$ and *Aclp*$^{HSC\text{-}KO}$ mice were fed a control diet (n = 6/group) or an HFC diet (n = 9/group) for 24 weeks. (A) (Left panel) Representative F4/80-immunostained liver samples. (Right panel) Quantification of hepatic F4/80 immunostaining. Scale bars: 25 μm. (B) Quantification of hepatic *Adgre1*, *Tnf*, and *Cd68* mRNA (n = 6/group). **p < 0.01 and *p < 0.05 vs. *Aclp*$^{fl/fl}$ mice fed a control diet for 24 weeks. p-values obtained via one-way ANOVA with Tukey's post-hoc test. Error bars represent the SEM.

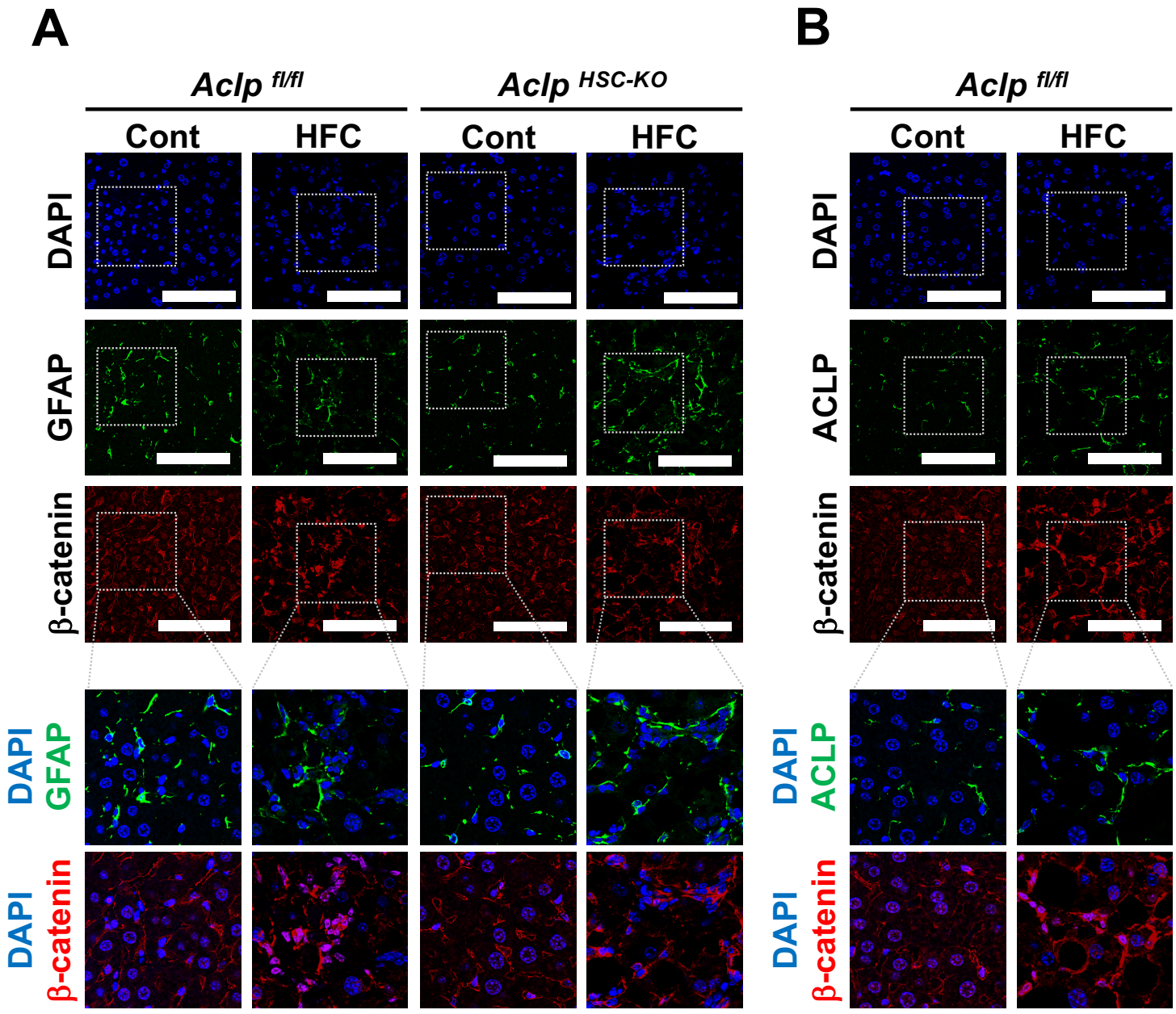


**Supplemental Figure 11. Immunofluorescence staining for β-catenin, GFAP, and ACLP in liver samples from murine models of NASH.**
(A and B) Eight-week-old male *Aclp*$^{fl/fl}$ and *Aclp*$^{HSC\text{-}KO}$ mice were fed a control diet (n = 6/group) or an HFC diet (n = 9/group) for 24 weeks. (A) (Upper panel) Representative images of immunofluorescence staining for β-catenin (red) and GFAP (green) in murine liver sections. The nuclei were stained with DAPI (blue). Scale bars: 100 μm. (Lower panel) β-catenin/nucleus co-stained sites are shown in purple. This figure is related to Figure 3B. (B) (Upper panel) Representative images of immunofluorescence staining for β-catenin (red) and ACLP (green) in murine liver sections. The nuclei were stained with DAPI (blue). Scale bars: 100 μm. (Lower panel) β-catenin/nucleus co-stained sites are shown in purple. This figure is related to Figure 3C.

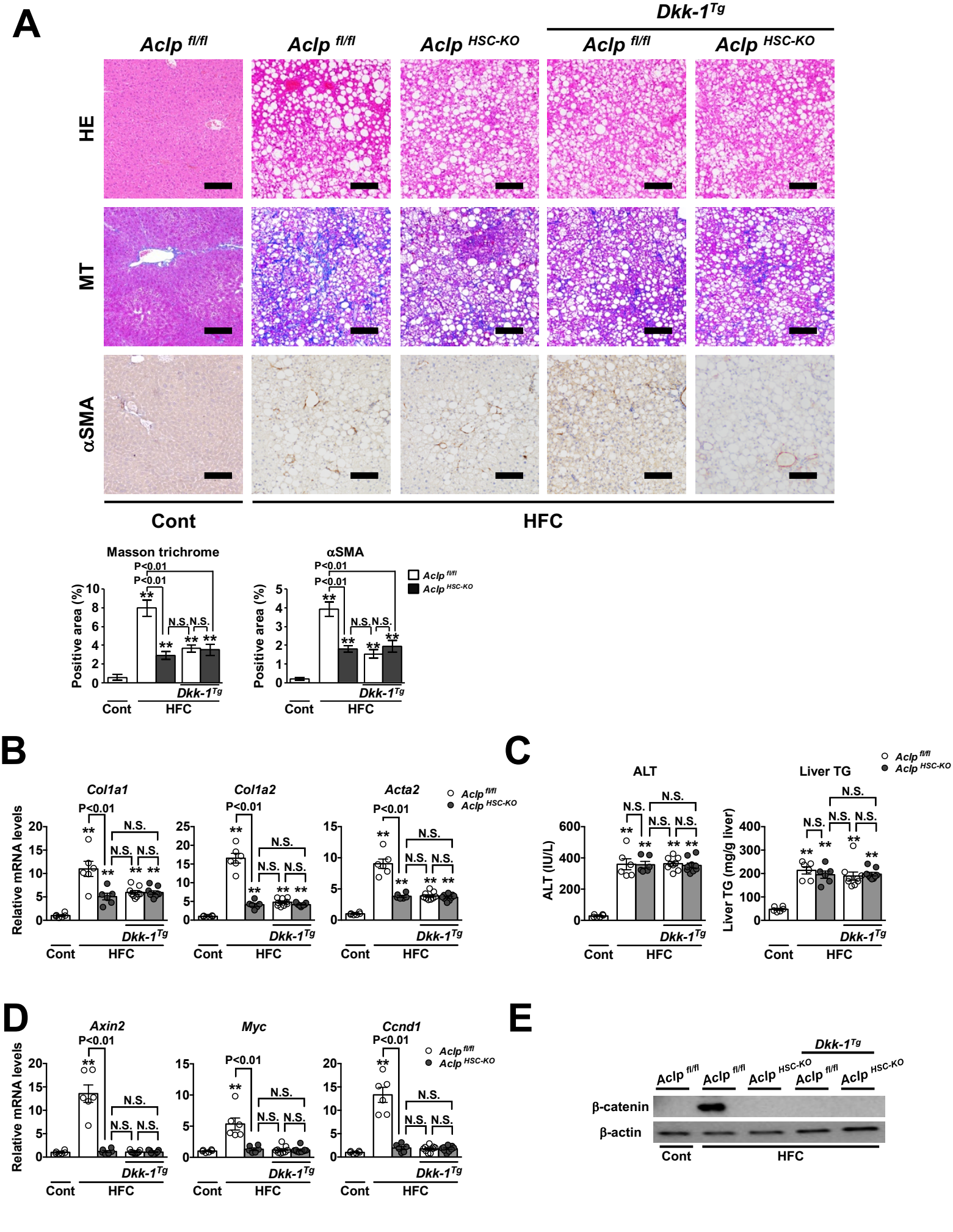
A
Aclp fl/fl
Aclp fl/fl
Aclp HSC-KO
Dkk-1Tg
Aclp fl/fl
Aclp HSC-KO
HE
MT
αSMA
Cont
HFC
Masson trichrome
Positive area (%)
P<0.01
P<0.01
N.S.
N.S.
Dkk-1Tg
Cont
HFC
αSMA
Positive area (%)
P<0.01
P<0.01
N.S.
N.S.
Aclp fl/fl
Aclp HSC-KO
Dkk-1Tg
Cont
HFC
B
Col1a1
Col1a2
Acta2
Relative mRNA levels
P<0.01
N.S.
Aclp fl/fl
Aclp HSC-KO
Dkk-1Tg
Cont
HFC
C
ALT
ALT (IU/L)
Liver TG
Liver TG (mg/g liver)
N.S.
Aclp fl/fl
Aclp HSC-KO
Dkk-1Tg
Cont
HFC
D
Axin2
Myc
Ccnd1
Relative mRNA levels
P<0.01
N.S.
Aclp fl/fl
Aclp HSC-KO
Dkk-1Tg
Cont
HFC
E
Dkk-1Tg
Aclp fl/fl
Aclp fl/fl
Aclp HSC-KO
Aclp fl/fl
Aclp HSC-KO
β-catenin
β-actin
Cont
HFC

**Supplemental Figure 12. ACLP expression in HSCs plays a major role in canonical WNT pathway activation in HSCs and in the resulting progression of liver fibrosis in murine NASH.**

(A–E) *Aclp*$^{fl/fl}$ mice (n = 6/group), *Aclp*$^{HSC\text{-}KO}$ mice (n = 6/group), *Aclp*$^{fl/fl}$*Dkk-1*$^{Tg}$ mice (n = 9/group), and *Aclp*$^{HSC\text{-}KO}$*Dkk-1*$^{Tg}$ mice (n = 9/group) were fed a control diet or an HFC diet for 24 weeks. (A) (Upper panel) Representative HE-stained, MT-stained, and αSMA-immunostained liver samples. Scale bars: 100 μm (HE-stained and MT-stained sections) and 50 μm (αSMA-immunostained sections). (Lower panel) Quantification of MT and αSMA staining. (B) Hepatic mRNA expression of *Col1a1*, *Col1α2*, and *Acta2*. (C) Serum ALT activity and hepatic TG level. (D) Quantification of *Axin2*, *Myc*, and *Ccnd1* mRNA in HSCs isolated from mice after being fed a control or an HFC diet for 24weeks. **p < 0.01 vs. *Aclp*$^{fl/fl}$ mice fed a control diet for 24 weeks. (E) Western blot for β-catenin accumulation in HSCs isolated from mice fed control or HFC diet for 24 weeks. p-values obtained via one-way ANOVA with Tukey's post-hoc test. Error bars represent the SEM.

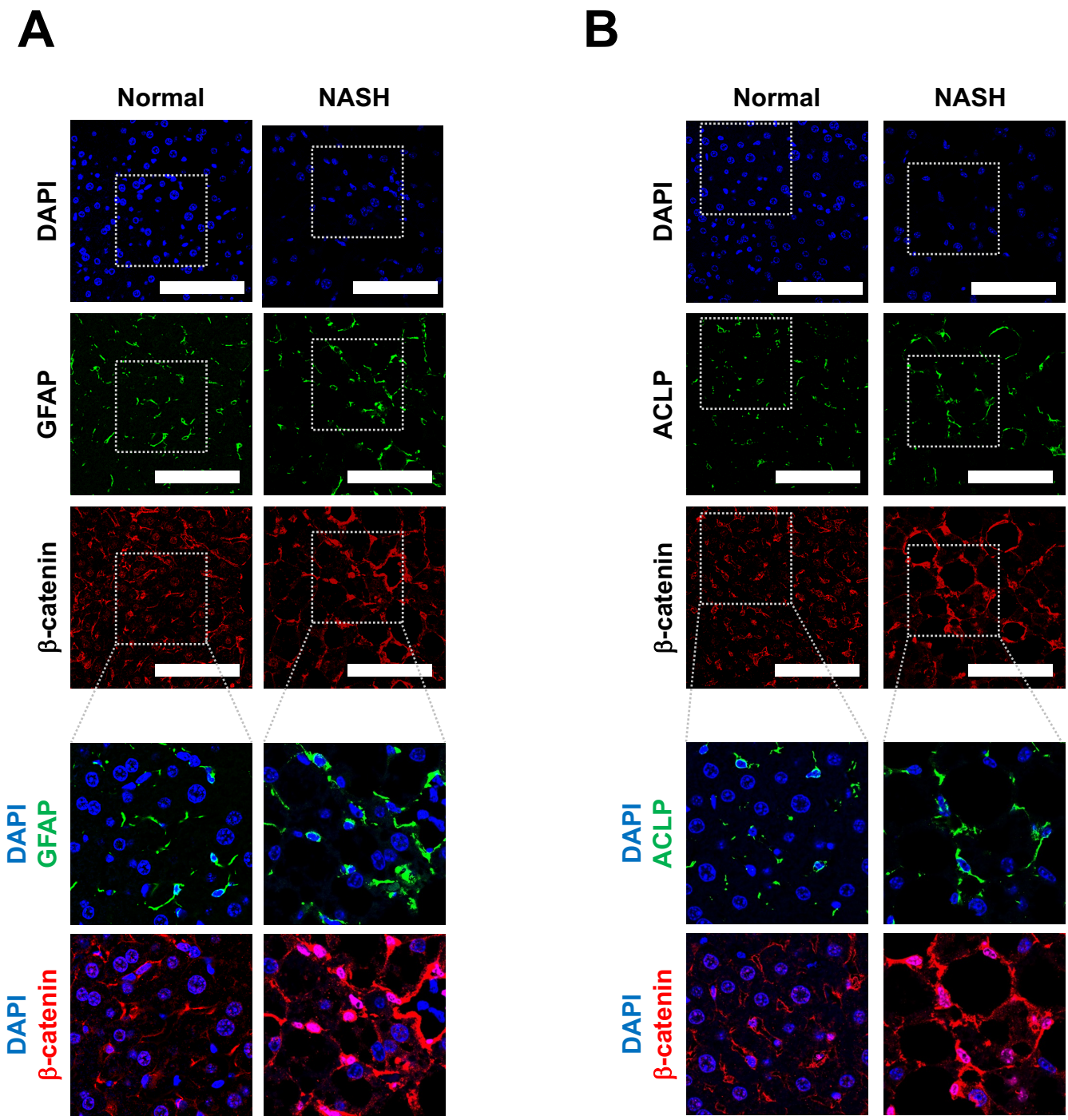


**Supplemental Figure 13. Immunofluorescence staining for β-catenin, GFAP and ACLP in liver samples of control subjects and NASH patients.**
(A and B) Liver sections from controls (n = 14) and NASH patients (n = 44) were used. (A) (Upper panel) Representative images of immunofluorescence staining for β-catenin (red) and GFAP (green) in human liver tissue samples. The nuclei were stained with DAPI (blue). Scale bars: 100 μm. (Lower panel) β-catenin/nucleus co-stained sites are shown in purple. This figure is related to Figure 3D. (B) (Upper panel) Representative images of immunofluorescence staining for β-catenin (red) and ACLP (green) in human liver tissue samples. The nuclei were stained with DAPI (blue). Scale bars: 100 μm. (Lower panel) β-catenin/nucleus co-stained sites are shown in purple. This figure is related to Figure 3D.

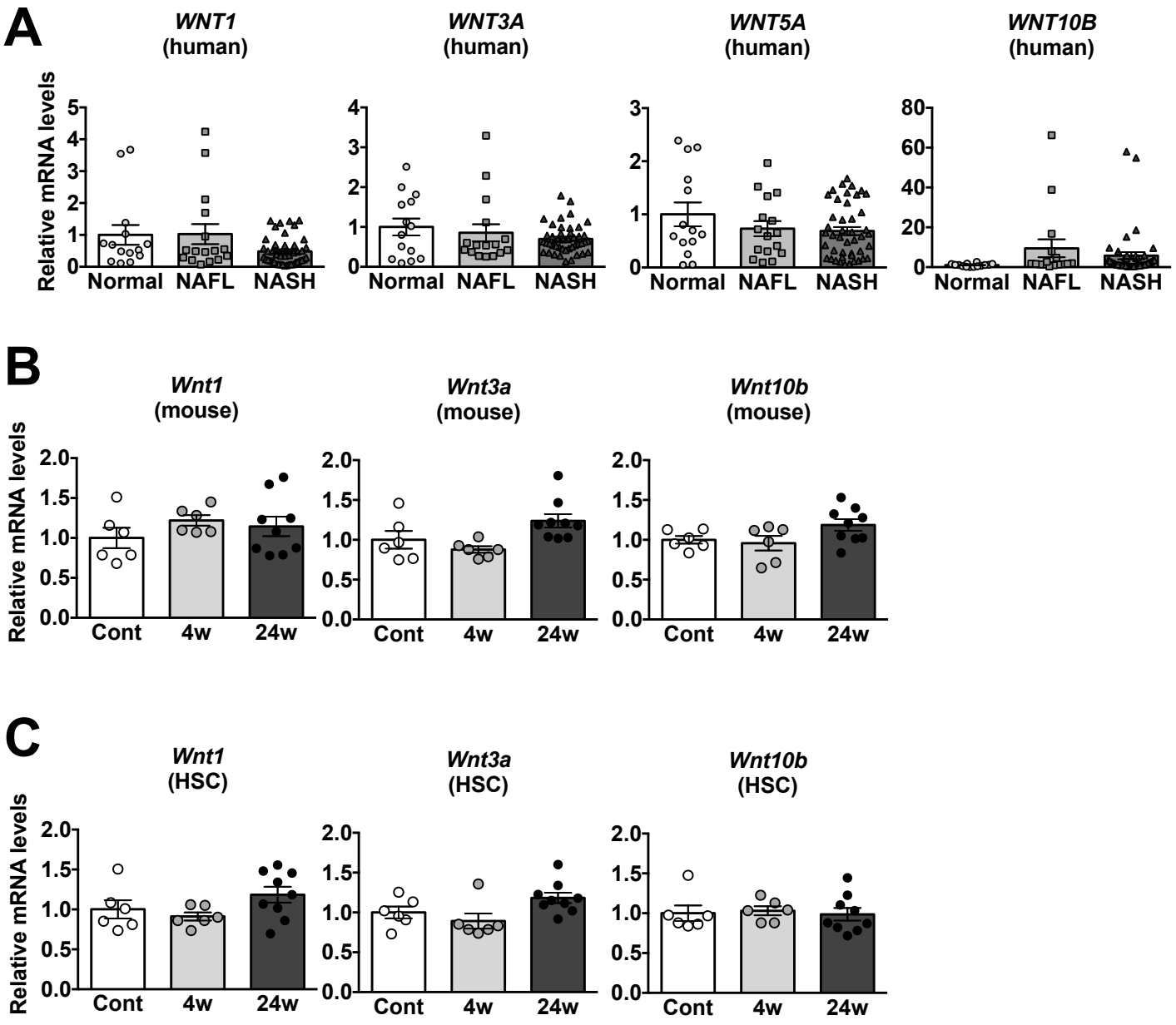


**Supplemental Figure 14. Quantification of WNT mRNA expression in liver samples from NAFLD patients and murine NAFLD models.**
(A) Quantification of *WNT1*, *3A*, *5A*, and *10B* mRNA expression in human liver samples from controls (n = 14), NAFL patients (n = 16), and NASH patients (n = 44). (B and C) Eight-week-old male *Aclp*$^{fl/fl}$ mice were fed an HFC diet for 4 weeks (n = 6/group) or 24 weeks (n = 9/group) to prepare murine NAFLD models or fed a control diet for 24 weeks (n = 6/group). (B) Hepatic expression of *Wnt1*, *3a*, and *10b* mRNA. Hepatic expression of *Wnt5a* mRNA could not be detected by qRT-PCR. (C) Quantification of *Wnt1*, *3a*, and *10b* mRNA expression levels in HSCs isolated from mouse livers. *Wnt5a* mRNA expression in HSCs could not be detected by qRT-PCR.

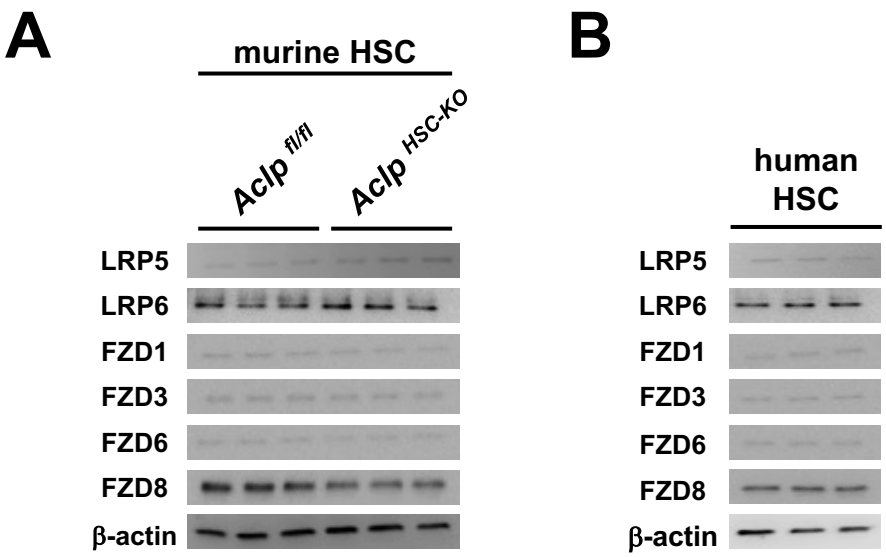


**Supplemental Figure 15. Western blot for LRP proteins and FZD proteins in murine and human HSCs.**
(A) Western blot for LRP5, LRP6, FZD1, FZD3, FZD6, and FZD8 expression in HSCs immediately after their isolation from *Aclp*$^{fl/fl}$ and *Aclp*$^{HSC\text{-}KO}$ mice (n = 3/group). (B) Western blot for LRP5, LRP6, FZD1, FZD3, FZD6, and FZD8 expression in human HSCs, immediately after their isolation from control subjects (n = 3).

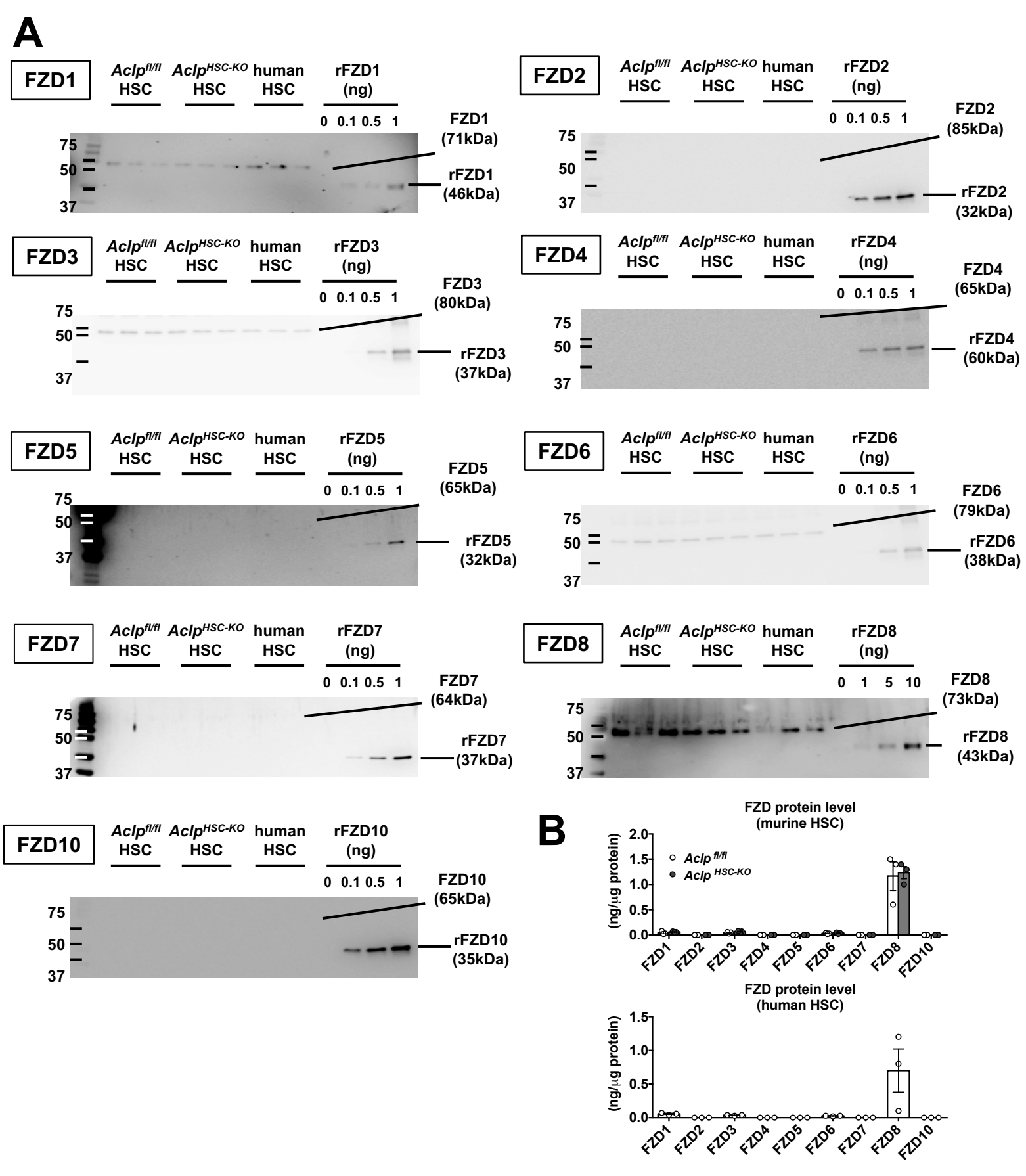


**Supplemental Figure 16. Quantification of FZD proteins in murine and human HSCs.**
(A) Western blot for FZD proteins in murine HSCs immediately after isolation from *Aclp*$^{fl/fl}$ and *Aclp*$^{HSC\text{-}KO}$ mice and in human HSCs immediately after isolation from control subjects (n = 3/group). Recombinant FZD proteins of known concentration were used to generate standard curves for the absolute quantification of endogenous FZD proteins in HSCs. (B) Quantification of FZD proteins in murine and human HSCs (n = 3/group).

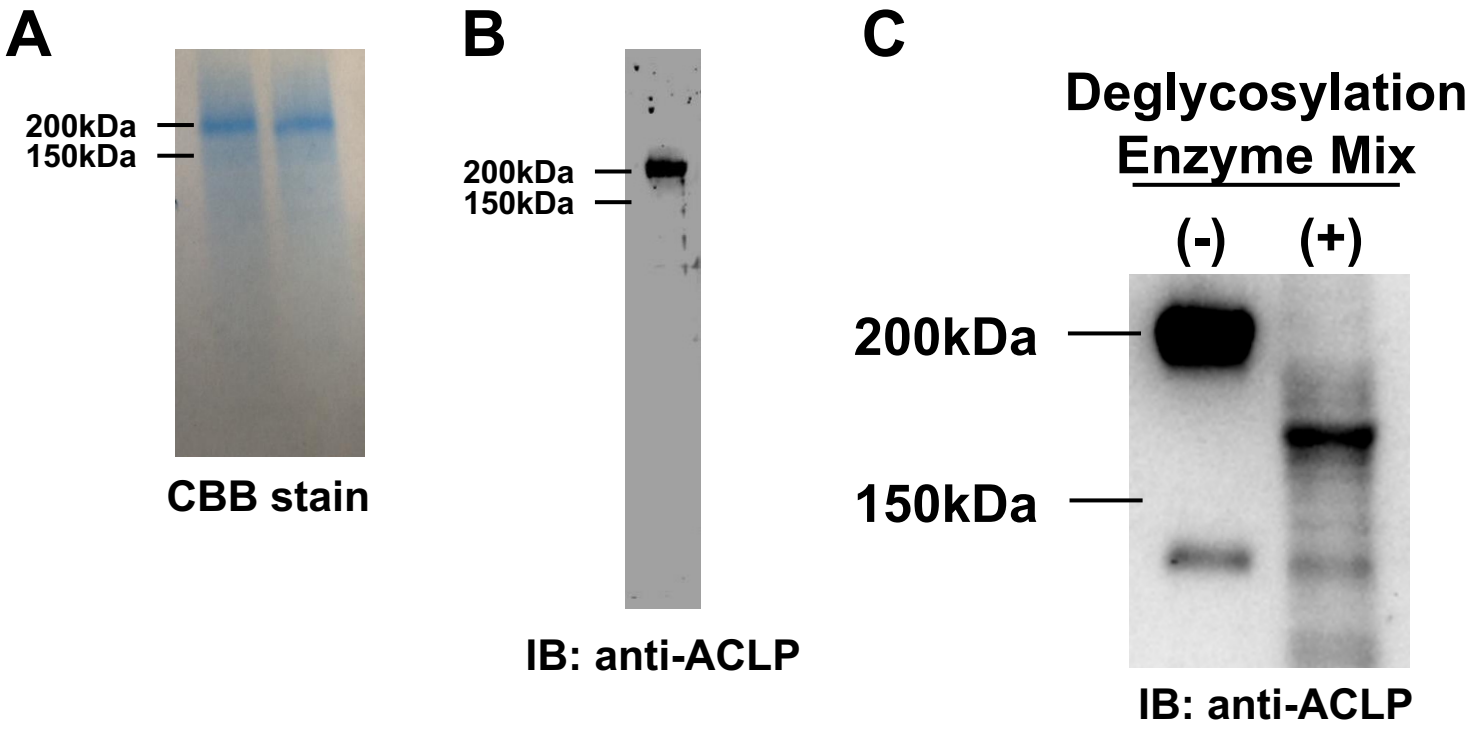


**Supplemental Figure 17. Purification of the recombinant mouse ACLP protein.**
(A) SDS-PAGE of the recombinant mouse ACLP (CBB staining). (B) Western blot for the recombinant mouse ACLP. (C) Deglycosylation of the recombinant mouse ACLP. The experiments were repeated three times.

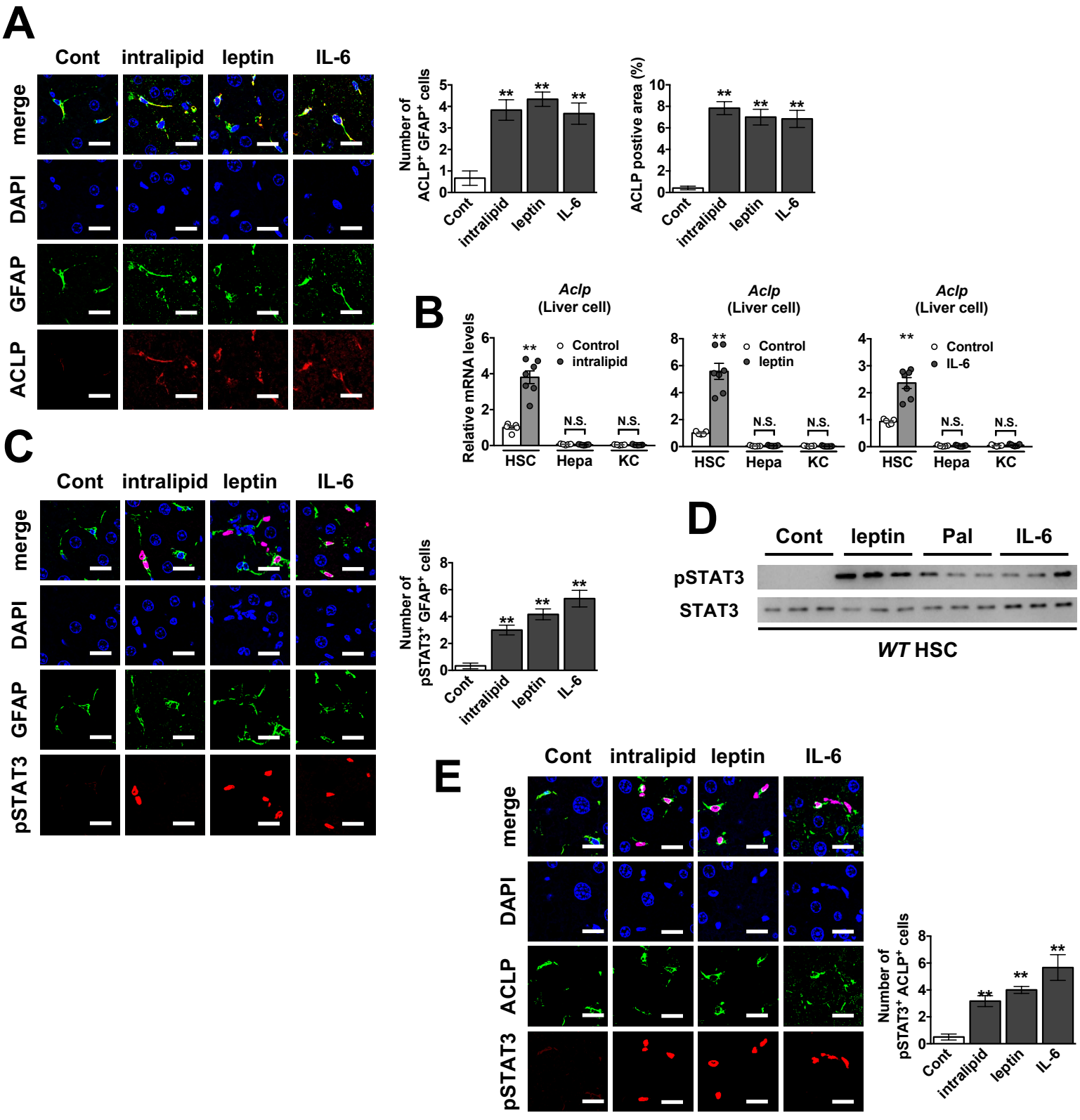


**Supplemental Figure 18. In vivo administration of obesity-related factors FFA, leptin, and IL-6 enhances ACLP expression in HSCs via activation of STAT3 signaling.** (A–E) Eight-week-old male wild-type mice were administered intralipid (n = 7/group), leptin (n = 7/group), IL-6 (n = 7/group), or PBS (n = 5/group). (A) (Left panel) Representative images of immunofluorescence double staining for ACLP (red) and GFAP (green) in the mouse liver samples at 4 hr after administration. Co-stained sites are shown in yellow. The nuclei were stained with DAPI (blue). Scale bars: 10 μm. (Right panel) Quantification of ACLP/GFAP double-positive cells, and quantification of ACLP staining. **p < 0.01 vs. control liver samples. (B) Quantification of *Aclp* mRNA expression levels in HSCs, hepatocytes, and Kupffer cells isolated from livers 4 hr after administration. **p < 0.01 vs. control group HSCs. (C) (Left panel) Representative images of immunofluorescence double staining for p-STAT3 (red) and GFAP (green) in the mouse liver samples at 4 hr after administration. The nuclei were stained with DAPI (blue). p-STAT3/nucleus co-stained sites are shown in purple. Scale bars: 10 μm. (Right panel) Quantification of p-STAT3/GFAP double-positive cells. **p < 0.01 vs. control liver samples. (D) Western blot for p-STAT3 and STAT3 protein expression in HSCs isolated from livers 30 min after administration. (E) (Left panel) Representative images of immunofluorescence double staining for pSTAT-3 (red) and ACLP (green) 4 hr after administration. The nuclei were stained with DAPI (blue). p-STAT3/nucleus co-stained sites are shown in purple. Scale bars: 10 μm. (Right panel) Quantification of pSTAT-3/ACLP double-positive cells. **p < 0.01 vs. control liver samples. p-values obtained via one-way ANOVA with Tukey's post-hoc test (A, C, and E) and unpaired Student's *t*-tests (B). Error bars represent the SEM.

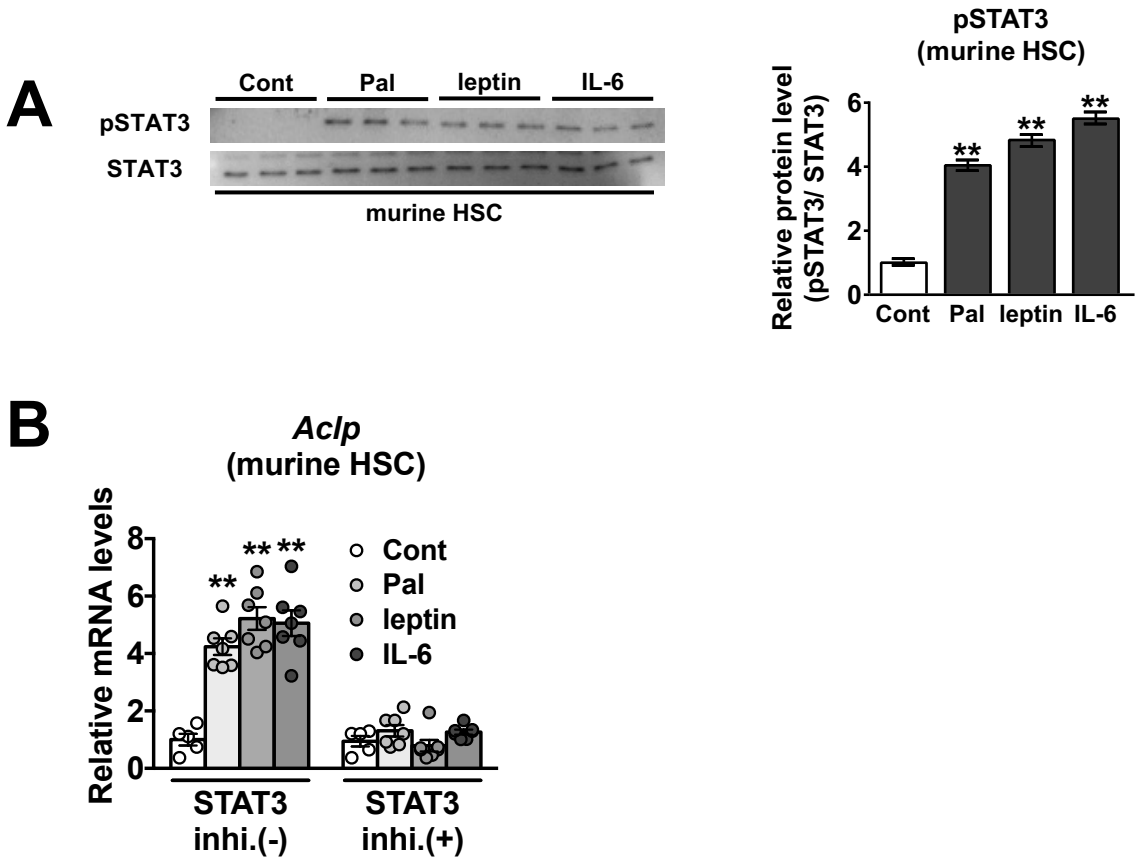


**Supplemental Figure 19. In vitro administration of obesity-related factors palmitate, leptin, and IL-6 enhances *Aclp* mRNA expression in murine HSCs via activation of STAT3 signaling.**

(A) Western blot for and quantification of STAT3 and p-STAT3 proteins in primary cultured murine HSCs treated with palmitate (200 μM), leptin (100 ng/ml), IL-6 (100 ng/ml), or PBS for 6 hr (n = 3/group). **p < 0.01 vs. control HSCs treated with PBS. (B) Quantification of *Aclp* mRNA expression in primary cultured murine HSCs treated with palmitate (n = 7/group), leptin (n = 7/group), IL-6 (n = 7/group), or PBS (n = 5/group) in the presence or absence of STAT3 inhibitor Stattic (2 μM) for 6 hr. **p < 0.01 vs. control HSCs treated with PBS in the absence of STAT3 inhibitor. p-values obtained via one-way ANOVA with Tukey's post-hoc test. Error bars represent the SEM.

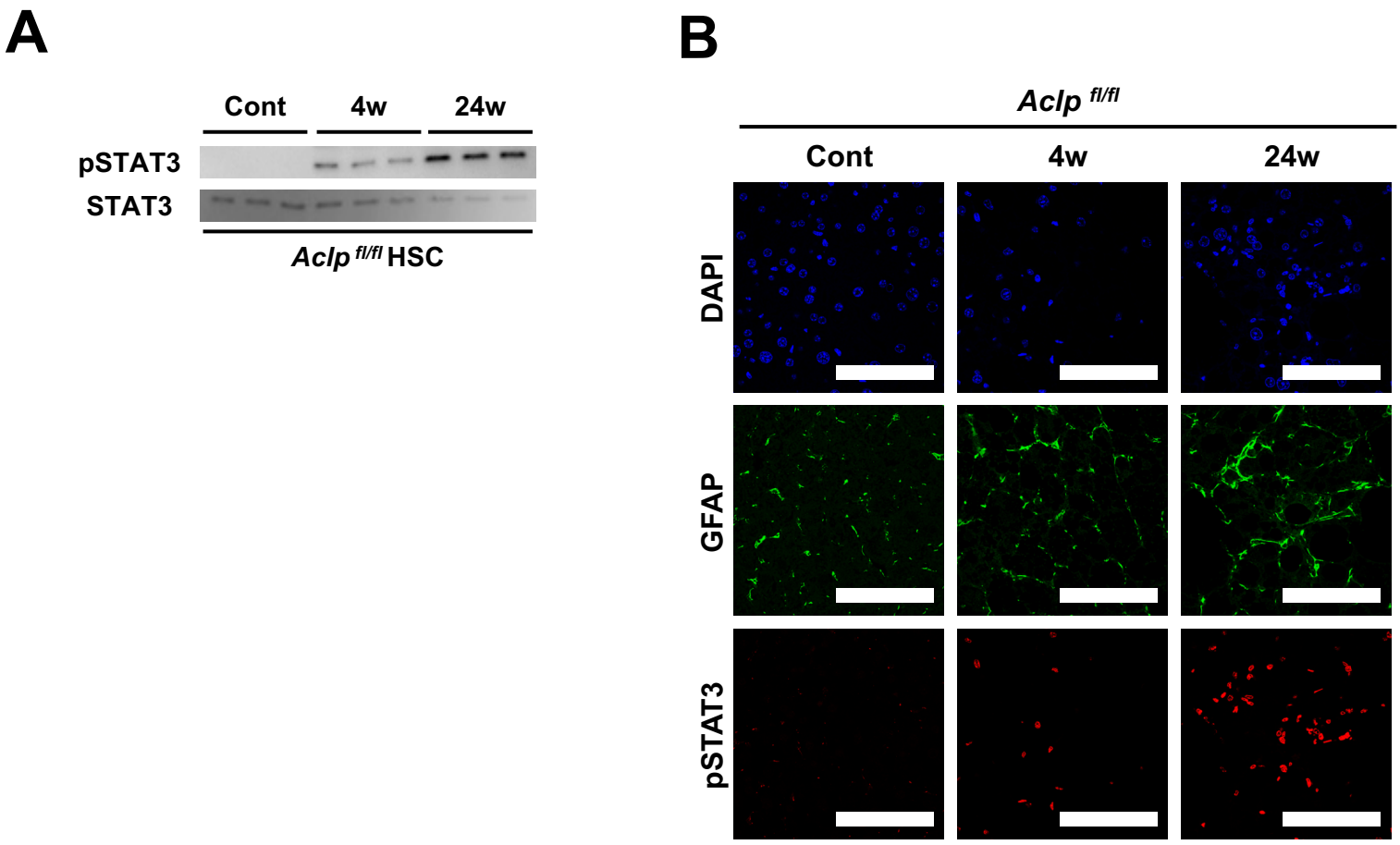


**Supplemental Figure 20. In livers of murine NAFLD models, p-STAT3 levels in HSCs increase with the progression of NAFLD.**
(A and B) Eight-week-old male *Aclp*$^{fl/fl}$ mice were fed an HFC diet for 4 weeks (n = 5/group) or 24 weeks (n = 7/group) to prepare a murine model of NAFLD, or a control diet for 24 weeks (n = 6/group). (A) Western blot for STAT3 and p-STAT3 protein expression in HSCs in control mice and murine models of NAFLD. (B) Representative images of immunofluorescence staining for p-STAT3 (red) and GFAP (green) in murine liver sections. Scale bars: 100 μm. The nuclei were stained with DAPI (blue). This figure is related to Figure 8D.

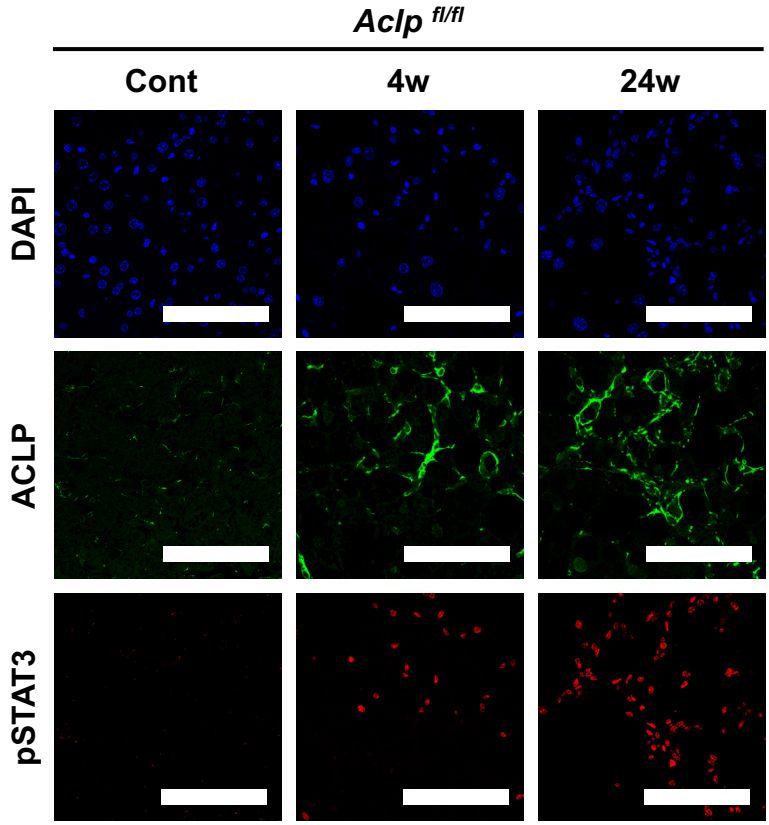


**Supplemental Figure 21. Immunofluorescence staining for p-STAT3 and ACLP in liver samples from murine models of NAFLD.**
Eight-week-old male *Aclp*$^{fl/fl}$ mice were fed an HFC diet for 4 weeks (n = 5/group) or 24 weeks (n = 7/group) to prepare a murine model of NAFLD, or a control diet for 24 weeks (n = 6/group). Representative images of immunofluorescence staining for p-STAT3 (red) and ACLP (green) in murine liver sections. Scale bars: 100 μm. The nuclei were stained with DAPI (blue). This figure is related to Figure 8E.

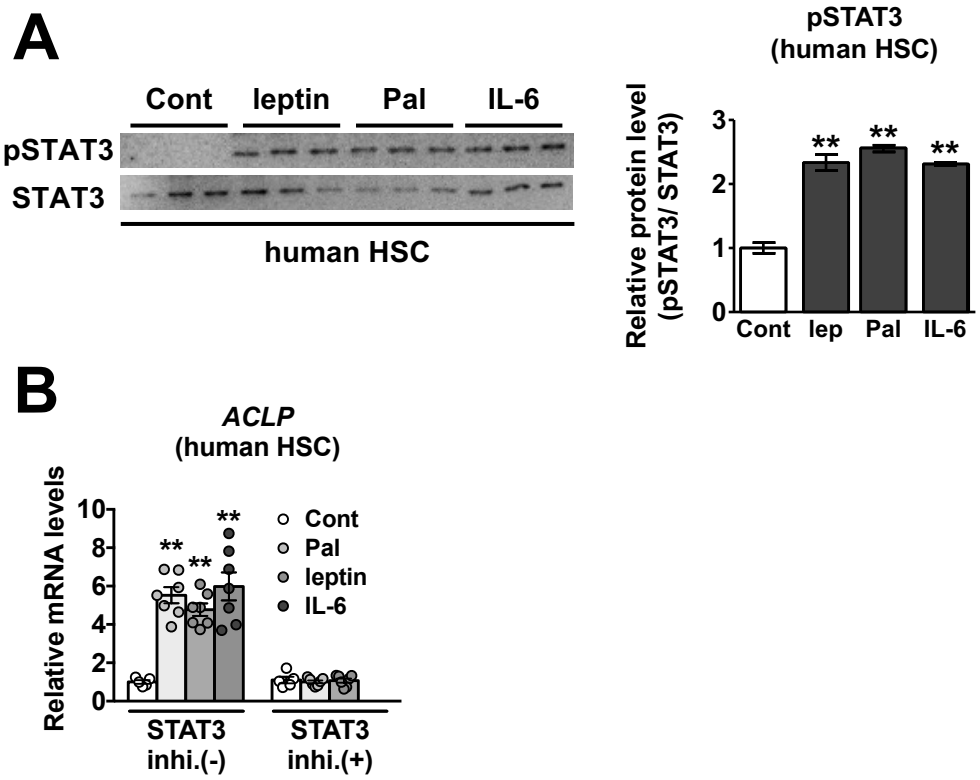


**Supplemental Figure 22. In vitro administration of obesity-related factors palmitate, leptin, and IL-6 enhances *ACLP* mRNA expression in human HSCs via activation of STAT3 signaling.**

Human primary cultured HSCs were isolated from control subjects and cultured. (A) Western blot for and quantification of STAT3 and p-STAT3 protein expression in human primary cultured HSCs incubated with palmitate (200 μM), leptin (100 ng/ml), IL-6 (100 ng/ml), or PBS for 6 hr. (B) Quantification of *ACLP* mRNA expression in human primary cultured HSCs incubated with palmitate (200 μM) (n = 7/group), leptin (100 ng/ml) (n = 7/group), IL-6 (100 ng/ml) (n = 7/group), or PBS (n = 5/group) for 6 hr in the presence of STAT3 inhibitor Stattic (2 μM) or not. **$p < 0.01$ vs. control HSCs treated with PBS in the absence of STAT3 inhibitor. p-values obtained via one-way ANOVA with Tukey's post-hoc test. Error bars represent the SEM.

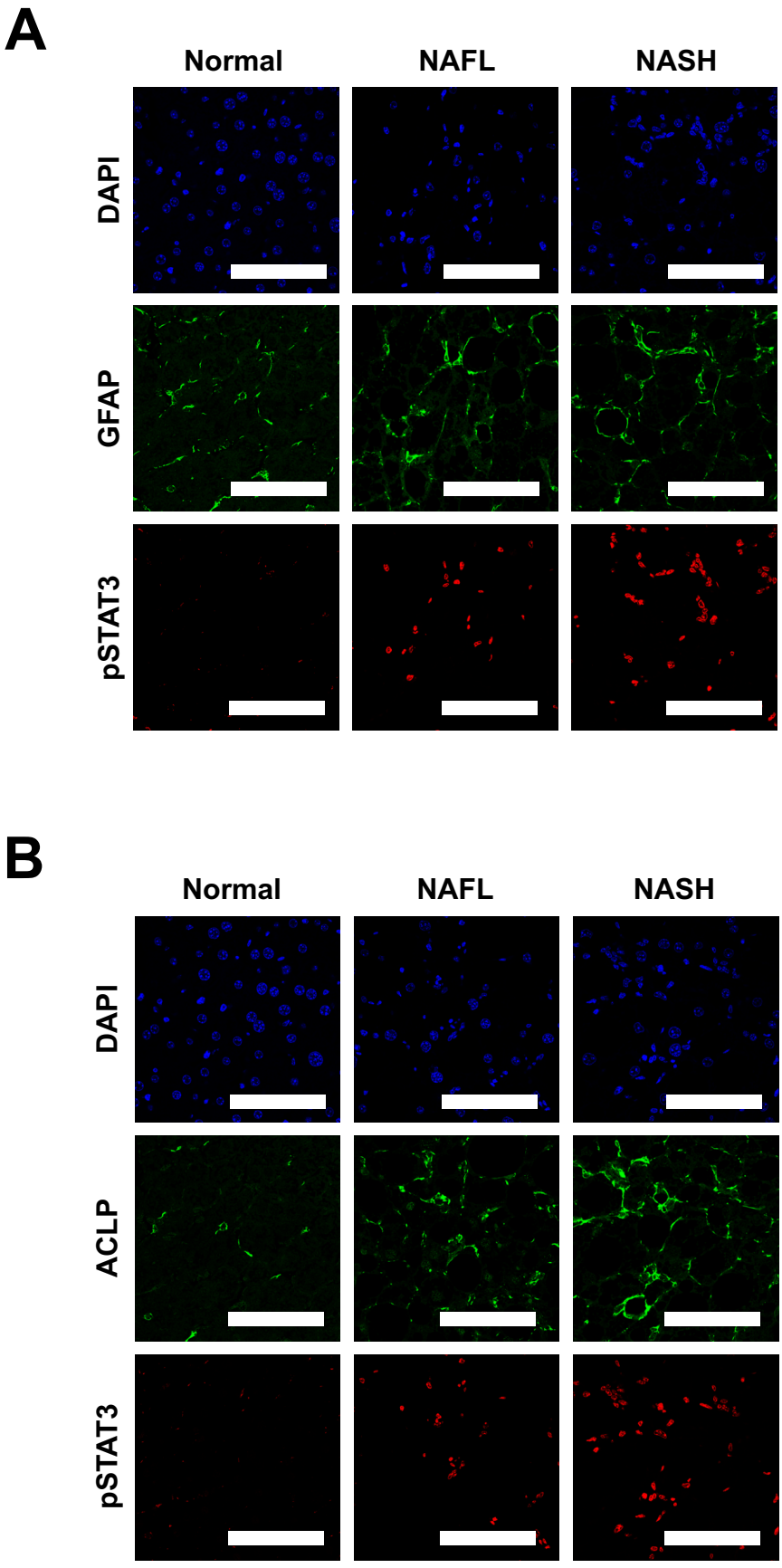


**Supplemental Figure 23. Immunofluorescence staining for pSTAT3, GFAP, and ACLP in liver samples from control subjects and NAFLD patients.**
(A and B) Liver sections from controls (n = 14), NAFL patients (n = 16), and NASH patients (n = 44) were used. (A) Representative images of immunofluorescence staining for p-STAT3 (red) and GFAP (green) in human liver tissue samples. The nuclei were stained with DAPI (blue). Scale bars: 100 μm. This figure is related to Figure 9B. (B) Representative images of immunofluorescence staining for p-STAT3 (red) and ACLP (green) in human liver tissue samples. The nuclei were stained with DAPI (blue). Scale bars: 100 μm. This figure is related to Figure 9C.

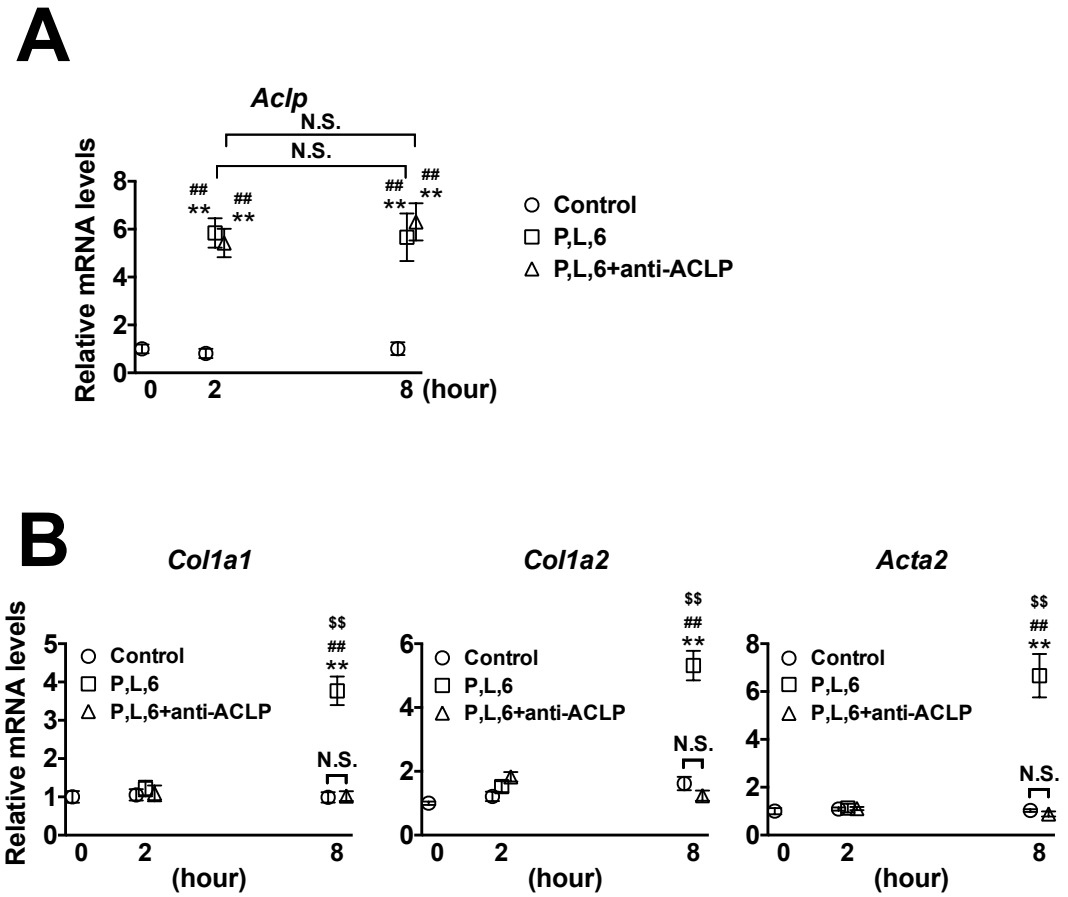


**Supplemental Figure 24. Increase in ACLP expression precedes the increase in fibrogenic gene expression during HSC activation after addition of mixture of palmitate, leptin, and IL-6, in vitro.**

Quantification of (A) *Aclp*, (B) *Col1a1*, *Col1a2*, and *Acta2* mRNA expression in murine primary cultured wild-type HSCs at the indicated time points after addition of mixture of palmitate (60 μM), leptin (30 ng/ml), and IL-6 (20 ng/ml) in the presence of anti-ACLP antibody (10 μg/ml) or not (n = 5/group). $^{**}p < 0.01$ vs. control HSCs before addition. $^{\#\#}p < 0.01$ vs. control HSCs at the indicated time point. $^{\$\$}p < 0.01$ vs. HSCs treated with palmitate, leptin, IL-6, and anti-ACLP antibody, at the indicated time point. p-values obtained via one-way ANOVA with Tukey's post-hoc test. Error bars represent the SEM.

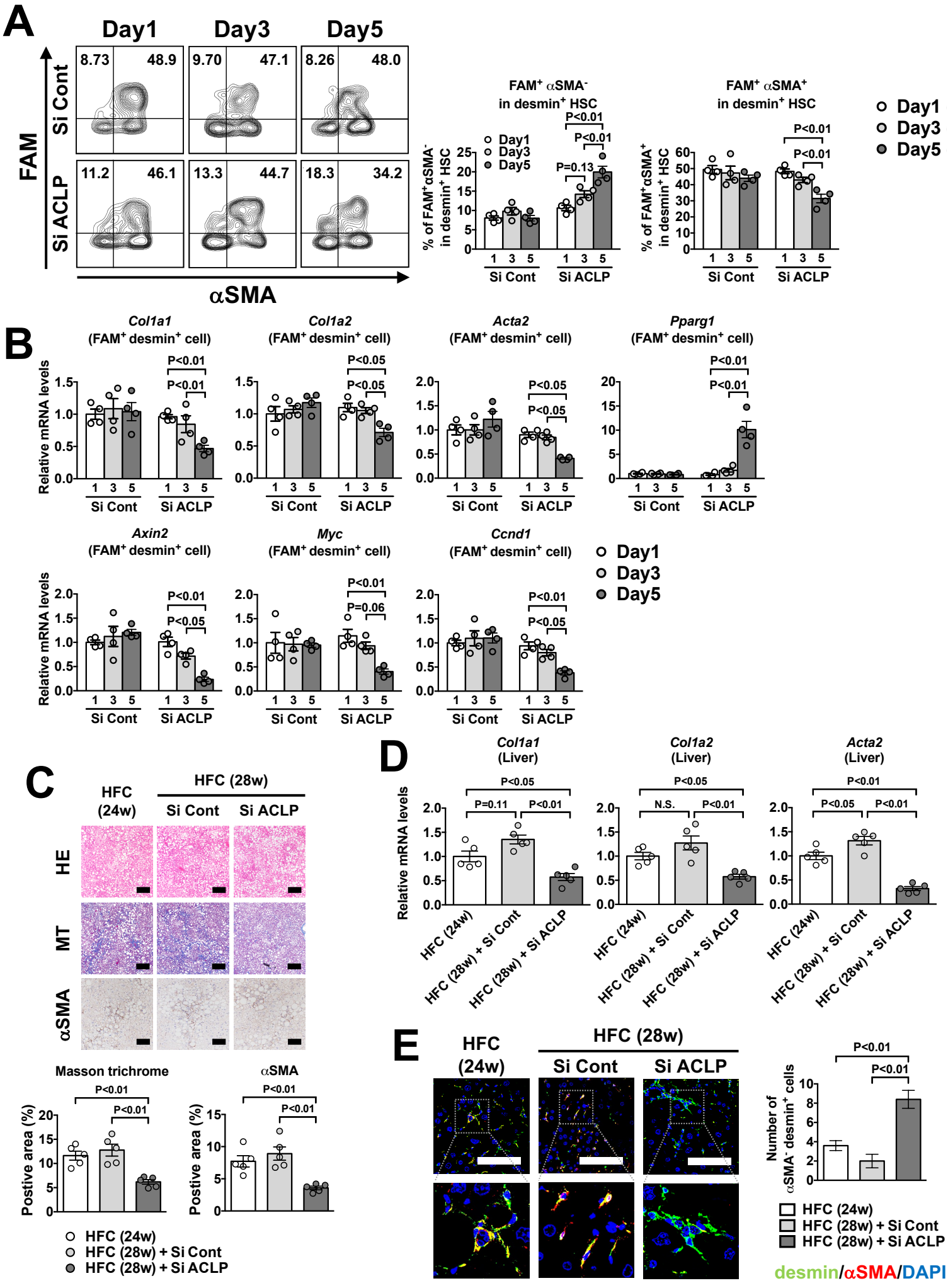
A
Day1
Day3
Day5
FAM
Si Cont
Si ACLP
αSMA
8.73
48.9
9.70
47.1
8.26
48.0
11.2
46.1
13.3
44.7
18.3
34.2
FAM+ αSMA- in desmin+ HSC
FAM+ αSMA+ in desmin+ HSC
% of FAM+αSMA- in desmin+ HSC
% of FAM+αSMA+ in desmin+ HSC
P<0.01
P=0.13
Si Cont
Si ACLP
B
Col1a1 (FAM+ desmin+ cell)
Col1a2 (FAM+ desmin+ cell)
Acta2 (FAM+ desmin+ cell)
Pparg1 (FAM+ desmin+ cell)
Axin2 (FAM+ desmin+ cell)
Myc (FAM+ desmin+ cell)
Ccnd1 (FAM+ desmin+ cell)
Relative mRNA levels
P<0.05
P=0.06
C
HFC (24w)
HFC (28w)
Si Cont
Si ACLP
HE
MT
αSMA
Masson trichrome
Postive area (%)
HFC (24w)
HFC (28w) + Si Cont
HFC (28w) + Si ACLP
D
Col1a1 (Liver)
Col1a2 (Liver)
Acta2 (Liver)
N.S.
E
Number of αSMA- desmin+ cells
desmin/αSMA/DAPI

**Supplemental Figure 25. Inhibition of ACLP in activated HSCs by administration of VA-lip-siRNA-ACLP reverses liver fibrosis in a murine NASH model.**
(A and B) Seven-week-old male wild-type mice were fed an HFC diet to prepare a murine model of NASH and, at 31 weeks of age, were concurrently injected through the tail vein with FAM-labeled VA-lip-siRNA-ACLP or VA-lip-siRNA-control (0.75 mg/kg body weight). HSCs were isolated from these mice at 1, 3, and 5 days after the injection, and analyzed by FACS (n = 4/group). (A) FACS analyses of $FAM^{+}\alpha SMA^{-}desmin^{+}$ HSC subsets and $FAM^{+}\alpha SMA^{+}desmin^{+}$ HSC subsets. (B) Quantification of *Col1a1*, *Col1a2*, *Acta2*, *Pparg1*, *Axin2*, and *Myc* mRNA expression in $FAM^{+}desmin^{+}$ HSCs sorted by FACS. (C–E) Seven-old male wild-type mice were fed an HFC diet for 28 weeks to prepare a murine model of NASH; from the 25th week, the mice were concurrently administered VA-lip-siRNA-ACLP or VA-lip-siRNA-control (0.75 mg/kg body weight) twice a week (n = 5/group). (C) (Upper panel) Representative HE-stained, MT-stained, and αSMA-immunostained liver samples. Scale bars: 100 μm (HE-stained and MT-stained sections) and 50 μm (αSMA-immunostained sections). (Lower panel) Quantification of MT staining and αSMA immunostaining. (D) Hepatic expression of *Col1a1*, *Col1a2*, and *Acta2* mRNA. (E) (Left panel) Representative images of immunofluorescence double staining of desmin (green) and αSMA (red) in murine liver sections. Co-stained sites are shown in yellow. The nuclei were stained with DAPI (blue). Scale bars: 100 μm. (Right panel) Quantification of $\alpha SMA^{-}desmin^{+}$ quiescent HSCs. p-values obtained via one-way ANOVA with Tukey's post-hoc test. Error bars represent the SEM.

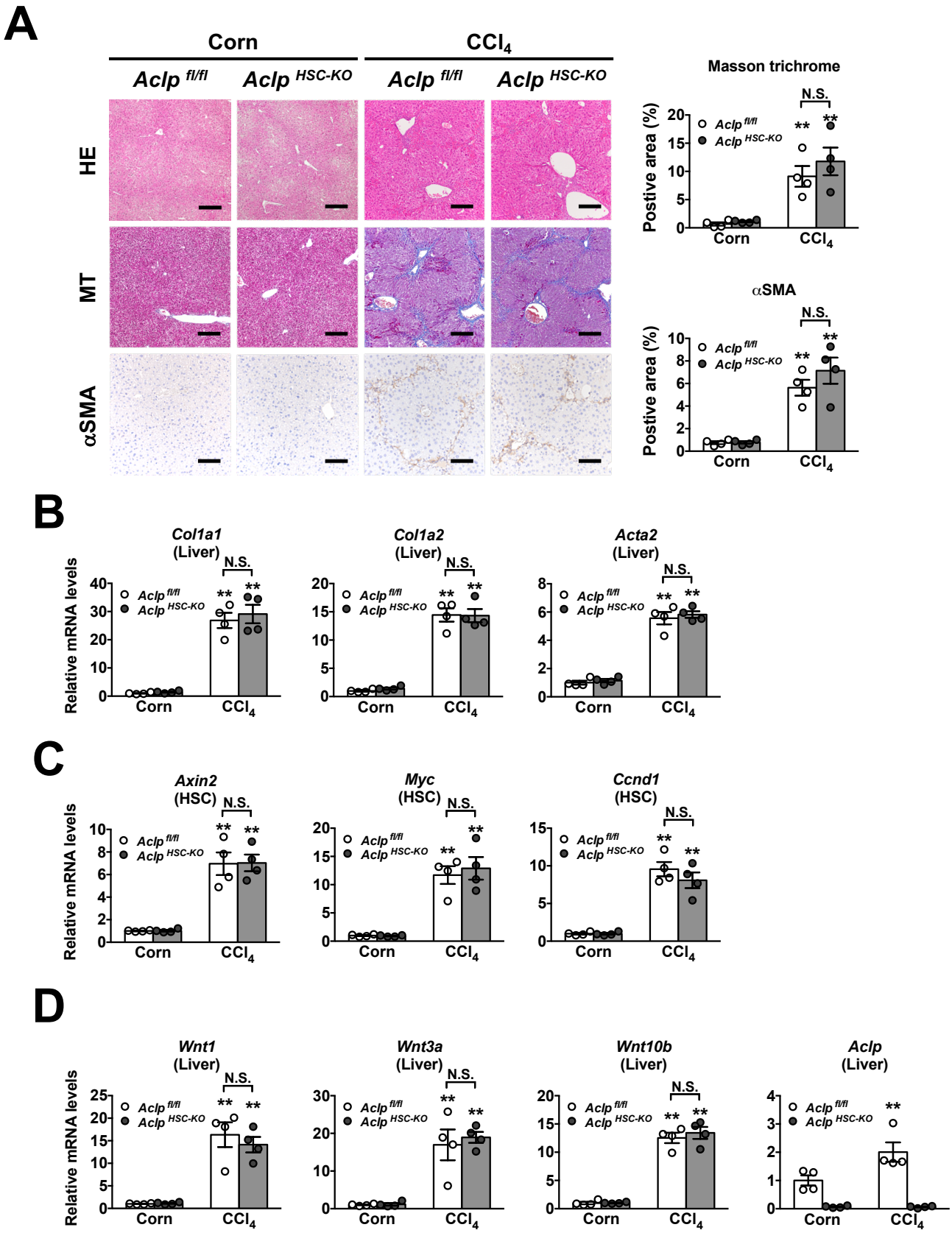


**Supplemental Figure 26. HSC-specific ACLP deficiency does not impact $CCl_4$-induced liver fibrosis in mice.**
(A–D) Eight-week-old male *Aclp*$^{fl/fl}$ and *Aclp*$^{HSC\text{-}KO}$ mice were treated with $CCl_4$ or corn oil, twice a week for 4 weeks (n = 4/group). (A) (Left panel) Representative HE-stained, MT-stained, and αSMA-immunostained liver samples. Scale bars: 200 μm (HE-stained and MT-stained sections) and 100 μm (αSMA-immunostained sections). (Right panel) Quantification of MT staining and αSMA immunostaining. (B) Hepatic expression of *Col1a1*, *Col1a2*, and *Acta2* mRNA. (C) Quantification of *Axin2*, *Myc*, and *Ccnd1* mRNA in HSCs isolated from mice in each group. (D) Hepatic expression of *Wnt1*, *Wnt3a*, *Wnt10b*, and *Aclp* mRNA. **p < 0.01 vs. *Aclp*$^{fl/fl}$ mice treated with corn oil. p-values obtained via one-way ANOVA with Tukey's post-hoc test. Error bars represent the SEM.

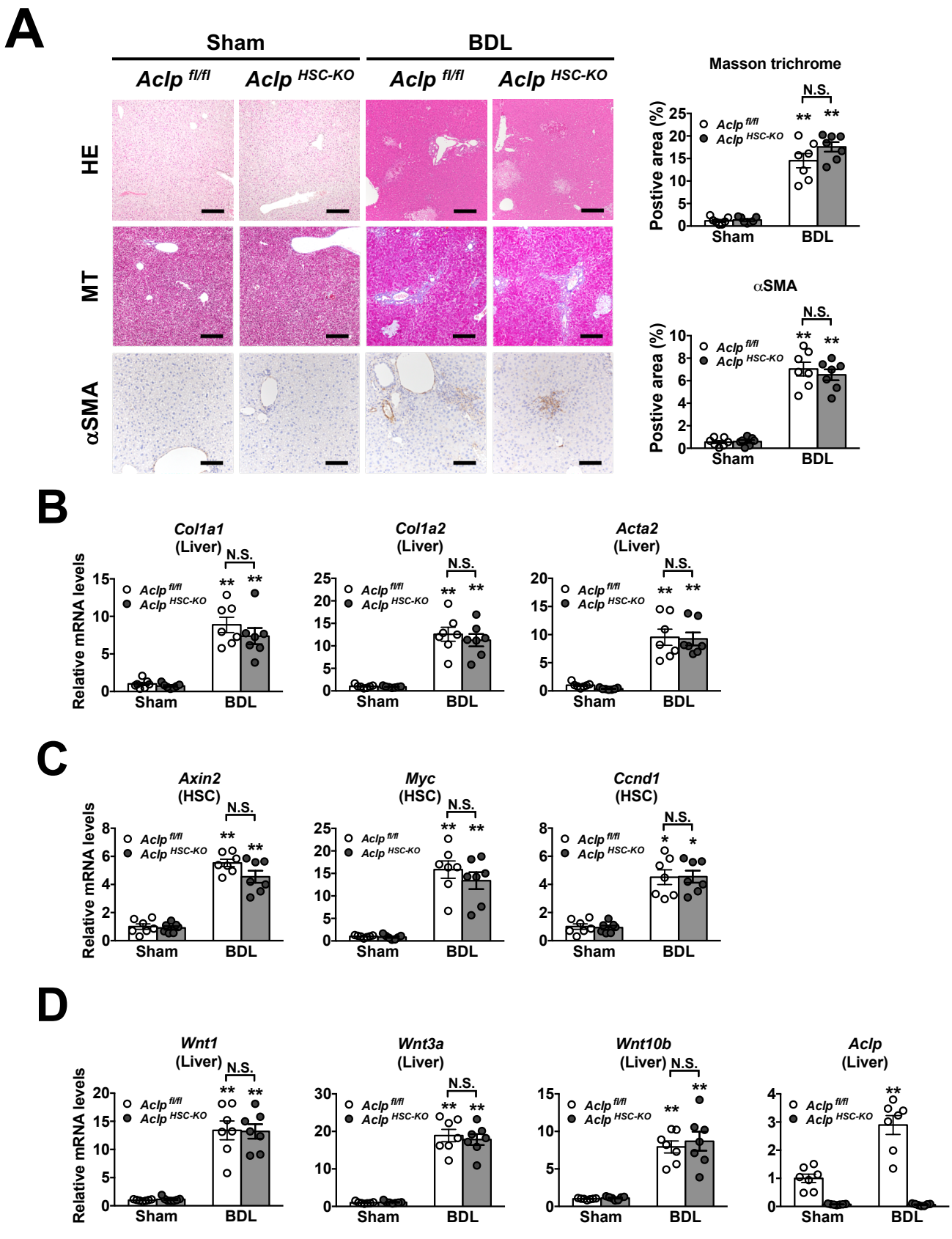


**Supplemental Figure 27. HSC-specific ACLP deficiency does not impact BDL-induced liver fibrosis in mice.**
(A–D) Eight-week-old male *Aclp*$^{fl/fl}$ and *Aclp*$^{HSC\text{-}KO}$ mice were subjected to BDL or sham operation for 3 weeks (n = 7/group). (A) (Left panel) Representative HE-stained, MT-stained, and αSMA-immunostained liver samples. Scale bars: 200 μm (HE-stained and MT-stained sections) and 100 μm (αSMA-immunostained sections). (Right panel) Quantification of MT staining and αSMA immunostaining. (B) Hepatic expression of *Col1a1*, *Col1a2*, and *Acta2* mRNA. (C) Quantification of *Axin2*, *Myc*, and *Ccnd1* mRNA in HSCs isolated from mice in each group. (D) Hepatic expression of *Wnt1*, *Wnt3a*, *Wnt10b*, and *Aclp* mRNA. **p < 0.01 vs. *Aclp*$^{fl/fl}$ mice subjected to the sham operation. p-values obtained via one-way ANOVA with Tukey's post-hoc test. Error bars represent the SEM.

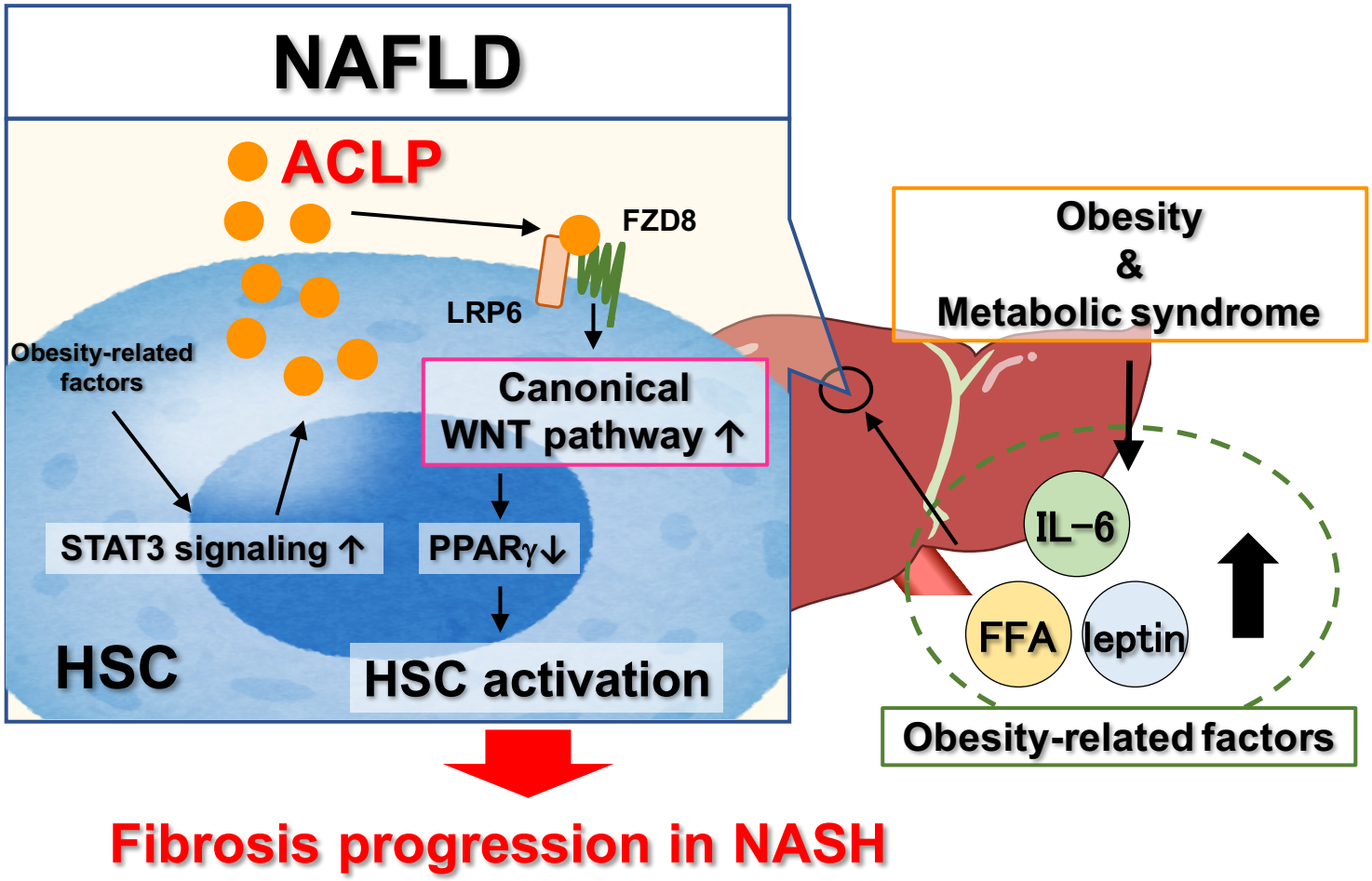


**Supplemental Figure 28. Roles of ACLP as a ligand in the canonical WNT pathway in the pathology of NASH.**

Supplemental Table 1: Antibody lists used in this study

| Primary antibodies | | | | | | | |
|---|---|---|---|---|---|---|---|
| name | vendor | product number | Origin | Clonality | Species reactivity | Application | dilution |
| anti-ACLP/AEBP1 antibody (H-164) | Santa Cruz Biotechnology | sc-32919 | rabbit | polyclonal | human | IHC | 1:50 |
| | | | | | | WB | 1:200 |
| | | | | | mouse | IHC | 1:50 |
| | | | | | | WB | 1:200 |
| anti-GFAP antibody | abcam | ab53554 | goat | polyclonal | human | IHC | 1:200 |
| | | | | | mouse | | |
| anti-GFAP antibody | Dako | Z0334 | rabbit | polyclonal | mouse | IHC | 1:500 |
| anti-desmin antibody | abcam | ab80503 | goat | polyclonal | human | IHC | 1:100 |
| | | | | | mouse | | |
| anti-beta catenin antibody [15B8] | abcam | ab6301 | mouse | monoclonal | human | IHC | 1:50 |
| | | | | | mouse | | |
| anti-beta catenin antibody | abcam | ab16051 | rabbit | polyclonal | human | WB | 1:400 |
| | | | | | mouse | | |
| anti-cytokeratin 19 antibody [A53-B] | abcam | ab194399 | mouse | monoclonal | human | IHC | 1:200 |
| | | | | | mouse | | |
| anti-phospho STAT3 (B-7) antibody | Santa Cruz Biotechnology | sc-8059 | mouse | monoclonal | human | IHC | 1:50 |
| | | | | | mouse | | |
| anti- phospho-STAT3 (Tyr705) antibody | Santa Cruz Biotechnology | sc-7993 | rabbit | polyclonal | human | WB | 1:200 |
| | | | | | mouse | | |
| anti-cre recombinase antibody [2D8] | Merck Millipore | MAB3120 | mouse | monoclonal | mouse | IHC | 1:1000 |
| anti-alpha smooth muscle actin antibody | abcam | ab5694 | rabbit | polyclonal | mouse | IHC | 1:50 |
| anti-F4/80 antibody [CI:A3-1] | AbD Serotec | MCA497 | rat | monoclonal | mouse | IHC | 1:50 |
| anti-FZD1 antibody [Clone # 162531] | R&D | MAB11201 | rat | monoclonal | human | WB | 1:1000 |
| | | | | | mouse | | |
| anti-FZD2 antibody | Sigma-Aldrich | SAB4501052 | rabbit | polyclonal | human | WB | 1:1000 |
| | | | | | mouse | | |
| anti-FZD3 antibody | abcam | ab217032 | rabbit | polyclonal | human | WB | 1:1000 |
| | | | | | mouse | | |
| anti-FZD4 antibody | Thermo Fisher Scientific | PA5-41972 | rabbit | polyclonal | human | WB | 1:1000 |
| | | | | | mouse | | |
| anti-FZD5 antibody | abcam | ab14475 | rabbit | polyclonal | human | WB | 1:1000 |
| | | | | | mouse | | |
| anti-FZD6 antibody | abcam | ab98933 | rabbit | polyclonal | human | WB | 1:1000 |
| | | | | | mouse | | |
| anti-FZD7 antibody | abcam | ab64636 | rabbit | polyclonal | human | WB | 1:1000 |
| | | | | | mouse | | |
| anti-FZD8 antibody [EPR7308(2)] | abcam | ab155093 | rabbit | monoclonal | human | WB | 1:1000 |
| | | | | | mouse | | |
| anti-FZD10 antibody | abcam | ab137491 | rabbit | polyclonal | human | WB | 1:1000 |
| | | | | | mouse | | |
| anti-LRP5 antibody [D5G4] | Cell Signaling Technology | #5440 | rabbit | monoclonal | human | WB | 1:1000 |
| | | | | | mouse | | |
| anti-LRP6 antibody [C47E12] | Cell Signaling Technology | #3395 | rabbit | monoclonal | human | WB | 1:1000 |
| | | | | | mouse | | |
| anti-Phospho-LRP6 (Tyr1492) antibody | Cell Signaling Technology | #2568 | rabbit | polyclonal | human | WB | 1:1000 |
| | | | | | mouse | | |
| anti-PPAR gamma antibody | abcam | ab59256 | rabbit | polyclonal | human | WB | 1:500 |
| | | | | | mouse | | |
| anti-lamin A/C antibody [EPR4100] | abcam | ab108595 | rabbit | monoclonal | human | WB | 1:10000 |
| | | | | | mouse | | |
| anti-STAT3 antibody [D3Z2G] | Cell Signaling Technology | #12640 | rabbit | monoclonal | human | WB | 1:1000 |
| | | | | | mouse | | |
| anti-beta-actin antibody [13E5] | Cell Signaling Technology | #4970 | rabbit | monoclonal | human | WB | 1:1000 |
| | | | | | mouse | | |
| anti-FLAG M2 antibody [Clone M2] | Sigma-Aldrich | F1804 | mouse | monoclonal | | WB | 1:400 |
| anti-human IgG antibody [EPR4421] | abcam | ab109489 | mouse | monoclonal | | WB | 1:1000 |
| anti-His-tag antibody | MBL | D291-3 | mouse | monoclonal | | WB | 1:500 |
| PE/Cy7-anti-CD45.2 antibody [clone: 104] | biolegend | 109829 | mouse | monoclonal | mouse | FACS | 1:100 |
| anti-alpha smooth muscle actin antibody [EPR5368] | abcam | ab202296 | rabbit | monoclonal | mouse | FACS | 1:100 |
| PE-anti-desmin antibody [DES/1711] | Novus Biologicals | NBP2-54503PE | rabbit | monoclonal | mouse | FACS | 1:100 |
| APC/Cy7-anti Thy-1.1 antibody [OX-7] | biolegend | 202519 | mouse | monoclonal | mouse | FACS | 1:100 |

| Secondary antibodies | | | | | | | |
|---|---|---|---|---|---|---|---|
| name | vendor | product number | Origin | Clonality | Species reactivity | Application | dilution |
| anti-rabbit IgG H&L (Alexa Fluor® 488) | abcam | ab150073 | donkey | polyclonal | rabbit | IHC | 1:500 |
| anti-rabbit IgG H&L (Alexa Fluor® 647) | abcam | ab150063 | donkey | polyclonal | rabbit | IHC | 1:500 |
| anti-goat IgG H&L (Alexa Fluor® 488) | abcam | ab150129 | donkey | polyclonal | goat | IHC | 1:500 |
| anti-mouse IgG H&L (Alexa Fluor® 647) | abcam | ab150107 | donkey | polyclonal | mouse | IHC | 1:500 |
| Histofine® Simple Stain™ Mouse MAX PO (rabbit) | Nichirei Bioscience | 414341F | | | rabbit | IHC | ready-to-use |
| Histofine® Simple Stain™ Mouse MAX PO (rat) | Nichirei Bioscience | 414311F | | | rat | IHC | ready-to-use |
| anti-rabbit IgG, HRP-linked whole antibody | GE Healthcare Life Sciences | NA934 | donkey | | rabbit | WB | 1:5000 |
| anti-rat IgG, HRP-linked whole antibody | GE Healthcare Life Sciences | NA935 | goat | | rat | WB | 1:5000 |
| anti-mouse IgG, HRP-linked whole antibody | GE Healthcare Life Sciences | NA931 | sheep | | mouse | WB | 1:5000 |
| anti-human IgG, HRP-linked whole antibody | GE Healthcare Life Sciences | NA933 | sheep | | human | WB | 1:5000 |